J. Fluid Mech. (1981), *vol.* 104, *pp.* 263–294
Printed in Great Britain

On the coherent structure of the axisymmetric mixing layer: a flow-visualization study

By A. K. M. F. HUSSAIN AND A. R. CLARK
Department of Mechanical Engineering, University of Houston, Texas 77004

(Received 1 July 1979 and in revised form 23 April 1980)

In an effort to resolve some controversies regarding the turbulent mixing-layer structure, the near field of a large (18 cm diameter) air jet has been investigated for the jet exit speed of $30\,\mathrm{m\,s^{-1}}$. The smoke-laden axisymmetric mixing layer has been illuminated by a thin sheet of laser light in an azimuthal plane passing through the jet axis. High-speed visualization films of the mixing layer in the region of its self-preservation (of which a few picture sequences depicting space–time evolutions of the structure of the layer are presented) reveal that most of the time the mixing layer is in a state of disorganization, consisting of relatively smaller scale, random and diffuse turbulent motions; only occasionally are organized distinct large-scale coherent structures formed. The survival distances of the large-scale structures are found to be comparable to their average sizes. The survival time of these structures is about one 'turnover' time, each being roughly about five times the local characteristic time scale of the mixing layer. It is seen that tearing is as dominant a mode of large-scale interaction as pairing is; large-scale structures are continually sheared and typically fragmented due to a segment on the high-speed side being torn and swept away from the slower-moving outer portion. Evolution of the large structures occur not primarily through complete pairing as widely believed but quite frequently through 'fractional pairing' between segments which have been torn from different upstream large-scale coherent structures or through 'partial pairing' when one structure captures only a part of another. The movies show that along with entrainment of non-vortical ambient fluid, radially outward ejection of vortical fluid into the ambient is an important aspect of jet mixing. From aligned displays of ciné film frame sequences, space–time trajectories of identifiable vortical fluid elements have been traced. The convection velocity variation across the shear layer and even the overall structure convection velocity measured from these trajectories agree with those determined from the wave-number–celerity spectra, obtained from double-Fourier transformation of longitudinal velocity space–time correlation measurements with hot-wires.

The visualization films do not bear out the two-street vortex ring model recently propounded by Lau. Based on our observations, we propose that tearing, 'slippage' and fractional and partial pairings are responsible for the observed radial variation of structure passage frequency, and the causes of the different coherent structures educed by Bruun on the high- and low-speed sides of the mixing layer and for Yule's failure in educing a coherent structure on the low-speed side of the layer.

0022–1120/81/4618–3290 $02.00

1. Introduction

Persistent suggestions have been made that turbulent shear flows are dominated by large-scale coherent structures which play the key role in transports of heat, mass and momentum, in entrainment (i.e. engulfment), and in aerodynamic noise generation. While the presence of large-scale motions in turbulent shear flows has been known for some time and occasionally investigated (Townsend 1956; Mollo-Christensen 1967; Kline *et al.* 1967; Phillips 1967; Landahl 1967; Kovasznay, Kibens & Blackwelder 1970), the current upsurge in research in this area has been triggered by the recent discovery of quasi-deterministic structures in flows that could be otherwise deemed fully (random) turbulent (Brown & Roshko 1974; Winant & Browand 1974; Crow & Champagne 1971; Hussain & Zaman 1975). While at relatively low Reynolds numbers, especially in the near fields of free turbulent shear flows, the existence of these structures have been conclusively demonstrated, we have had lingering doubt about their nature, even occurrence, at high Reynolds numbers; hence the motivation for this study. In fact, Chandrsuda *et al.* (1978) suggest that the roller-type Brown–Roshko structure is rare and a relic of upstream transition and will be three-dimensional in the presence of high free-stream or initial turbulence; see also Batt (1978) and Pui & Gartshore (1978). Yule (1978) claims that the axisymmetric turbulent mixing-layer structure is three-dimensional, but the outer side is diffuse and disorganized while the inner side of the eddies possess 'a reasonable degree of spatial and temporal coherence'.

Another motivation for this study stemmed from the recent hypothesis propounded by Lau (1978) that the near field of a circular jet consists of two coaxial streets of toroidal vortex rings bifurcating at $x/D \cong 1{\cdot}5$ from a single upstream street: 'the main vortex street' accelerating and converging on the jet axis at two potential core-lengths and 'the branch vortex street' decelerating and diverging from the jet axis. This provocative suggestion, even though inferred from extensive data, and intended to explain the large radial variation in structure passage frequency (Ko & Davies 1971; Lau & Fisher 1975; Bruun 1977; Clark 1979), appeared to us to be quite unconvincing and in need of investigation. A flow-visualization study appeared to be the only direct avenue for obtaining conclusive evidence regarding the nature of the coherent structures in the mixing layer. Another reason for using the visualization method was to supplement the more popular controlled perturbation and conditional sampling studies. While controlled excitation studies (Hussain & Zaman 1977; Zaman & Hussain 1980; Hussain & Thompson 1980; Sokolov *et al.* 1980) provide the convenience of educing the details of the coherent structure through phase-lock onto the induced perturbation, these were either performed typically in a low-Reynolds-number flow (Oster *et al.* 1977) or there was doubt that the induced structures were not representatives of naturally occurring structures (Lau 1978). On the other hand, eduction of naturally occurring structures through the application of conditional sampling suffers from a number of constraints because of the random variation in the formation time, shape, size, orientation, strength and convection velocity of the structures. A description of the coherent structure will involve multiple probes, and the eduction will be prohibitively time consuming (Hussain, Kleis & Sokolov 1980). There is also ambiguity regarding the criteria for detection of the naturally occurring coherent structure in the mixing layer. Bruun (1977) has shown that the educed characteristics and the convection velocity of natural structures in an axisymmetric mixing layer

depend significantly on whether the detection is triggered on positive or negative spikes of the u-signal. While triggering on the negative peaks of the u-signal on the high-speed side, Yule (1978) was unable to educe any structure on the low-speed side.

Even though the hot-wire is the most common tool employed for quantitative investigations in turbulent flows, flow-visualization is very effective in obtaining clearer preceptions of the physical phenomena and in the planning of sophisticated quantitative measurements; flow-visualization has at times even served to settle disputes concerning the interpretation of data. For these reasons, supplementation of quantitative data by visual studies is progressively becoming somewhat of a standard approach in large-scale structure studies in turbulence – a kind of rebirth, as most early fluid mechanics investigations relied heavily on flow-visualization. Indeed, it appears that flow-visualization has become practically indispensable to the understanding and characterization of the coherent structures in turbulent shear flows (Kline *et al.* 1967; Corino & Brodkey 1969; Rockwell 1972; Brown & Roskho 1974; Winant & Browand 1974; Browand & Laufer 1975; Bruun 1977; Yule 1978; Oster *et al.* 1977; Petersen 1978; Liepmann 1978). It appears that the present study constitutes the highest-Reynolds-number flow at which structures have been visualized in detail.

It is necessary to clarify that references made to the plane mixing layer in this paper are not intended to suggest similarity between this layer and the axisymmetric mixing layer. Clearly, unlike the plane mixing layer, the axisymmetric mixing layer has an imposed length scale, namely the jet diameter, D. Consequently, for sufficiently far downstream, say for $x/D \gtrsim 1$, the diameter, in addition to the distance ($\cong x$) from the virtual origin, also enters as a length scale. However, sufficiently close to the jet lip, i.e. $x/D \ll 1$, the axisymmetric mixing-layer characteristics should not be different from those of the plane mixing layer – provided that $\theta_e/D \ll 1$; θ_e is the exit shear layer momentum thickness. Thus, comparison with the plane mixing layer is strictly meaningful only for $x/D \gtrsim 1$. However, some integral measures of the axisymmetric mixing layer have been compared with those of the plane mixing layer for two reasons: (i) the latter flow has been more extensively studied, while available data in the axisymmetric mixing layer are extremely limited (Hussian & Husain 1980; Birch 1980, private communication), and (ii) there is an amazing similarity between the average measures of the axisymmetric layer until the end of the potential core and the plane player (Husain & Hussain 1979; Foss 1977).

2. Apparatus and procedures

The jet facility used for this study is located in a fairly large laboratory ($30 \times 10 \times 4$ m) with controlled temperature, humidity and traffic so that influences of recirculation draft and ambient turbulence (Kotsovinos 1976; Bradshaw 1977) are not likely to be significant. The centrifugal blower is driven by a d.c. motor operated by an in-house built (full-wave rectifier) controller which can hold the blower speed constant over long runs. The facility consists of a number of wooden and sheet metal modules connected together by flexible rubber couplings. The blower–motor assembly is vibrationally isolated from the laboratory floor. Following the blower are acoustic dampers, a square diffuser, a square-to-round conversion box, a 5 m long 75 cm diameter settling chamber followed by a 1·3 m long fibreglass nozzle of a compromise Batchelor–Shaw/

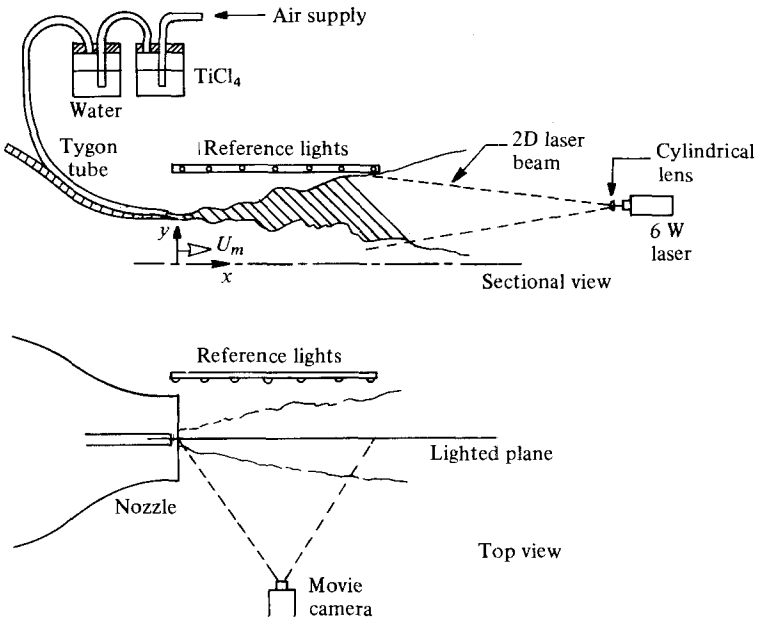

FIGURE 1. Schematic diagram of the flow field.

cubic equation profile (contraction ratio 18:1). The diffuser and settling chamber are fitted with a number of screens of 12 mesh/cm. The exit longitudinal turbulence intensity is 0·25 %. The outside of the nozzle exit is bevelled to a sharp lip so that the primary and entrained (from stagnant ambient) flows merge at an angle of 20° (see figure 1). Because of the heavy build and modular construction, the nozzle and laboratory floor are free from any perceptible vibration.

This study focuses on the high-speed flow-visualization of the mixing layer, achieved after a number of experimentations with lighting and still and ciné cameras. The flow was made visible by means of titanium dioxide smoke injected about 5 mm upstream of the nozzle exit on the low-speed (i.e. outer) side of the mixing layer through a 1 cm Tygon tube pressed into an elliptic shape. Note that the smoke is injected at an extremely small speed ($\cong 0{\cdot}5\ \mathrm{m\ s^{-1}}$), considerably lower than even the local entrainment speed, so that the smoke stream does not constitute a jet interacting with the mixing layer. The smoke merely oozes out as a laminar stream and is entrained into a thin laminar sheet (of about 2 mm thickness) near the jet lip. Consequently, the smoke merely passively marks the shear layer and the smoke stream does not alter the initial boundary-layer state, otherwise inevitable with smoke injection directly into the flow stream. This method of smoke injection was found to be optimum after trials with various alternatives.

Various lighting and camera techniques were also experimented with before the final choice. These included: single-exposure still pictures with stroboscopic lighting which produced blurred smoke boundaries even at the highest shutter speed; high-speed movies with floodlighting which produced faint images with the fastest available film; and movies with spot-lighting which revealed very little of the mixing-layer details due to averaging along the line of sight. The last step produced pictures which indicated presence of some coherent structures, but the mixing-layer boundaries

appeared quite blurred. It became apparent that a better picture of the sectional view of the mixing layer could be obtained by illuminating a thin transverse slice of the layer with a high-intensity planar light, easily obtained with a laser beam. We were cognizant of the limitation of the technique of illumination in a thin slice: changes in the smoke-marked fluid boundaries may not be completely attributable to flow evolution, but may be partly due to azimuthal fluid motion. Nevertheless, we chose this visualization technique because of its relative superiority over the alternatives. As discussed later, events like pairing, tearing, slippage, etc. inferred from the picture sequences including those shown here, are not confused noticeably by azimuthal motions, because the evolutionary changes are faster and quite distinctly identifiable in contrast with changes attributable to azimuthal motion.

A 6 W Spectra-physics (model 165) argon-ion laser, located at about 5 m downstream from the nozzle exit, was used to illuminate a thin radial plane passing through the middle of the Tygon tube. A cylindrical lens was used to obtain a thin sheet (about 2 mm wide) of intense light from the laser operated in the multiline mode (so that maximum total light intensity available was utilized). Kodak Ektachrome VNX video film (no. 7250) in conjunction with a Fastax (Model WF3) high-speed 16 mm ciné camera was used at a rate of 2000 pictures/s corresponding to a single-frame exposure time of 160 μs. The film speed, which has to start from zero, varies over most of the 30 m long film. Thus, for time reference, timing marks were placed on the film at 10 ms intervals by a Millitime timing-mark generator. These timing marks were subsequently used to determine the time δt elapsed between successive frames in the movie sequence as well as determine the convection velocity of coherent structures.

Three camera positions were used to film the flow. The streamwise ranges of the flow captured from these three positions were 7–43 cm, 23–59 cm, and 7–64 cm. In each case, the line of sight was located perpendicular to the illuminated plane at the midpoint of the streamwise range of the flow covered. In order to provide a streamwise length reference, a series of incandescent lights were mounted 5·08 cm apart on a blackened metal strip which was suspended sufficiently above and behind the lighted plane so as not to influence the flow perceptibly. Because the illumination is in a plane quite different from that of the reference lights, the corresponding scales for length in the visualization plane were corrected for the parallax effect. The reference length of 5·08 cm between two adjacent lights must be multiplied by 0·82 for the first two camera positions (i.e. for x-ranges 7–43 and 23–59 cm) and 0·88 for the third (i.e. for the x-range 7–64 cm).

3. Results and discussion

3.1. *Mean characteristics of the mixing layer*

Before examining the coherent structures, it is necessary to characterize the mixing-layer mean features. These characteristics, obtained from hot-wire measurements, include the initial condition, namely the efflux boundary-layer characteristics as well as the evolution of its integral measures like distributions of mean velocity, turbulence intensities, Reynolds stress, spectrum, spread rate, virtual origin, etc. In particular, it is interesting to see whether or not the mixing layer achieved a state of self-preservation within the range of visualization.

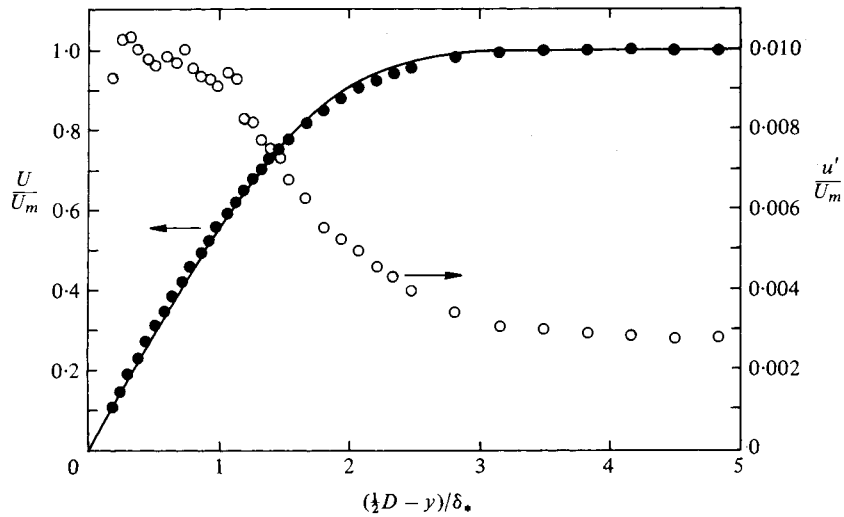

FIGURE 2. Longitudinal mean and fluctuation intensity profiles in the initial condition; ——, Blasius profile.

(*a*) *Initial condition.* The characteristics of the efflux boundary layer were measured at $x \cong 1$ mm, i.e. slightly downstream from the lip (see figure 1). The profiles of longitudinal mean velocity U/U_m and turbulence intensity u'/U_m at this initial condition are shown in figure 2. The y-location of the wall was determined from a linear extrapolation of the mean velocity data for $U/U_m < 0{\cdot}4$. Note that the distance $y' = \frac{1}{2}D - y$ from the wall is non-dimensionalized by the displacement thickness

$$\delta_* \equiv \int_0^\infty (1 - U/U_m)\, dy',$$

where U_m is the maximum mean velocity (i.e. the core value of U). The mean velocity profile $U(y')$ agrees quite well with the Blasius profile shown in figure 2 for comparison. The boundary-layer thickness δ (corresponding to $U/U_m = 0{\cdot}99$) was determined via a least-squares polynomial fit of the data in the outer part of the boundary layer. Values of δ_* and the momentum thickness

$$\theta = \int_0^\infty (U/U_m)(1 - U/U_m)\, dy'$$

were calculated by integrating U/U_m data via Simpson's rule. At the reference initial state (i.e. $x = 1$ mm), the values of δ, δ_*, and θ were found to be 2·48, 0·76, and 0·31 mm, respectively. The shape factor $\delta_*/\theta = 2{\cdot}53$ agrees well with the Blasius value 2·59 within the experimental uncertainty. One reason for the high value of the longitudinal fluctuation intensity in the initial condition is that measurements were made downstream of the lip, and the scatter is due to inadequate integration time.

(*b*) *Evolution characteristics of the mixing layer.* The streamwise evolutions of the profiles of longitudinal mean velocity, $U(y)$, r.m.s. longitudinal and transverse fluctuation velocities $u'(y)$ and $v'(y)$, and Reynolds stress $\overline{uv}(y)$ are shown in figures 3(*a*)–(*d*), respectively. Apart from depicting the details of progresive spreading of the shear layer, these figures also show that the peaks of fluctuation intensities and Reynolds

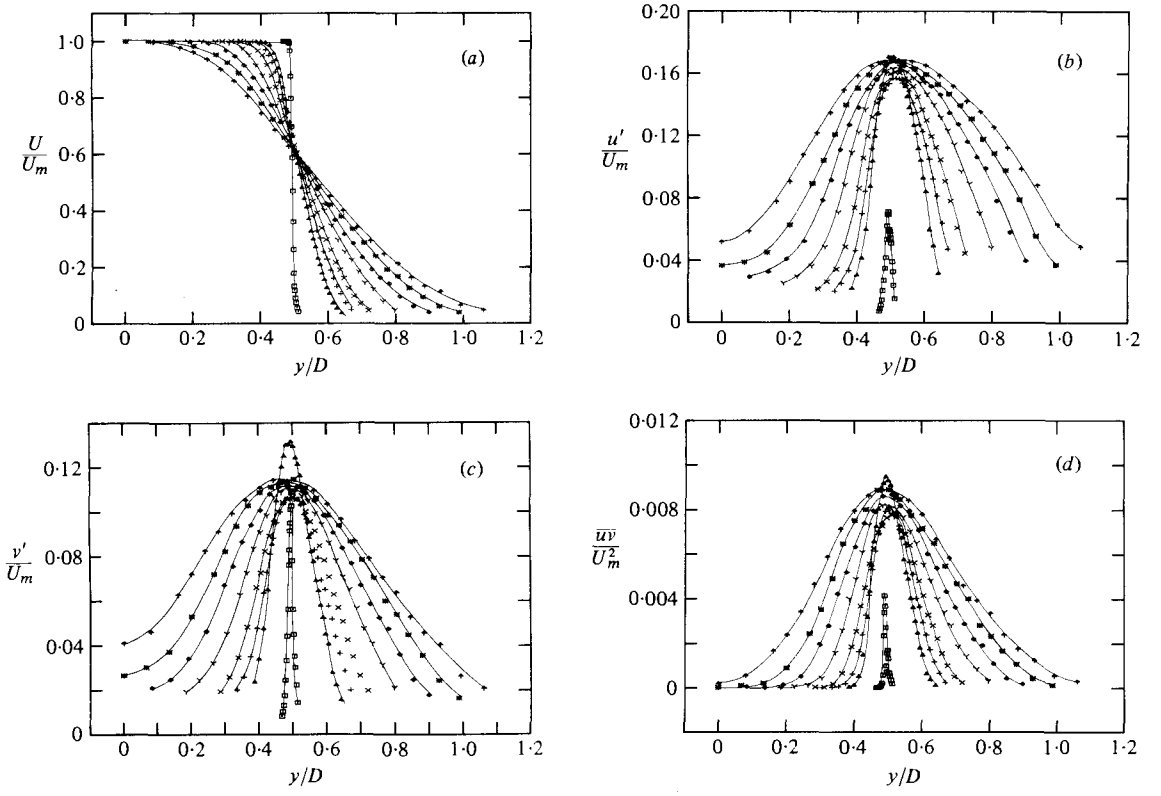

FIGURE 3. Streamwise evolutions of profiles of (*a*) U, (*b*) u', (*c*) v', (*d*) $\overline{uv}$. x/D values are: □, 0·14; △, 0·71; +, 1·06; ×, 1·41; Y, 2·12; ◇, 2·82; *, 3·53; ⩚, 4·23.

stress first increase rapidly to high values, presumably due to preferred location of the roll-up of the initially laminar layer, then rapidly drop before gradually increasing to their asymptotic constant values. Compared to these trends, initially turbulent layers show significantly retarded growth of the peak values (Bradshaw 1966; Hussain & Zedan 1978; Clark 1979). Note that figures 3(*a*)–(*d*) show that the time-average potential core extends beyond the last station, i.e. $x/D = 4{\cdot}23$. In order to test the achievement of self-preservation, data in the last four stations are replotted in figures 4(*a*)–(*d*) as functions of $(y - y_{0{\cdot}5})/\theta_{0{\cdot}1}$, where

$$\theta_{0{\cdot}1} = \int_{y_{0{\cdot}1}}^{\infty} (U/U_m)(1 - U/U_m)\, dy'$$

is the local momentum thickness of the shear layer; $y_{0{\cdot}5}$ and $y_{0{\cdot}1}$ are the transverse locations where U/U_m is 0·5 and 0·1, respectively. Note that the profile integration is terminated on the low-speed side at the y-location where $U/U_m = 0{\cdot}1$ in order to avoid the effects of entrainment-induced transverse mean velocity as well as high fluctuation intensity and, in particular, flow reversal (Hussain & Zaman 1980). Note that congruence of the profiles is the best for $U(y)$ and comparatively worst for $\overline{uv}(y)$. Thus, similarity is achieved earliest for $U(y)$, and progressively farther downstream for the profiles of $u'(y)$, $v'(y)$ and $\overline{uv}(y)$, in sequence. Note that the fluctuation intensities

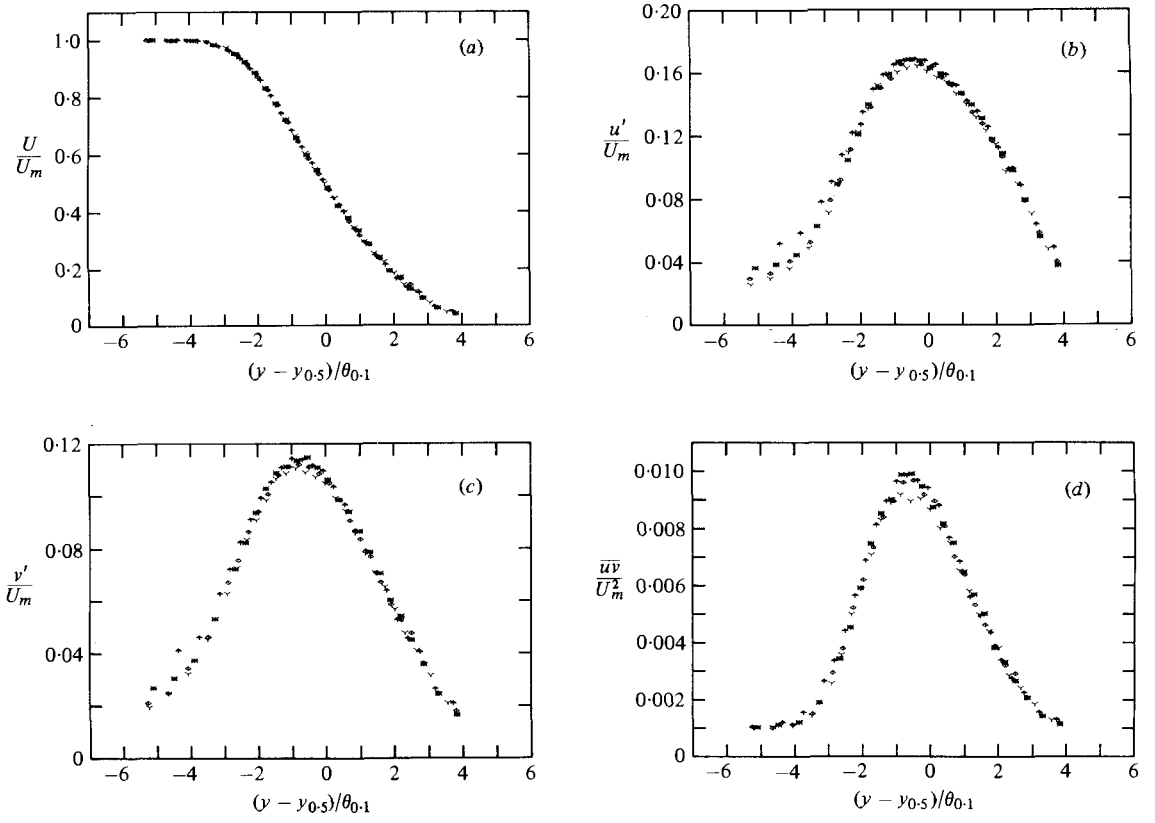

FIGURE 4. Self-preservation profiles of (*a*) U, (*b*) u', (*c*) v', (*d*) $\overline{uv}$. For legend see figure 3.

increase with x on the jet core side due to increasing flow fluctuations as the end of the potential core is approached. However, these fluctuations are mostly potential and should not contribute to the Reynolds stress $\overline{uv}$, as is clear from figure 4(*d*). The scatter in the u', v', $\overline{uv}$ profiles can be reduced with increased averaging time. The larger scatter in $\overline{uv}$ indicates that the integration time is not sufficiently large compared to the time scale of the Reynolds-stress-producing motions. Note that, because of the progressive increase of the flow time scale with x, the integration time must also increase with x.

The mean boundaries of the mixing layer are shown in figures 5(*a*). The lines connecting the constant values of $F = U/U_m$ show that the spread of the layer is linear beyond $x \simeq 0{\cdot}70D$. The streamwise evolution of the mixing-layer momentum thickness $\theta_{0.1}$ is shown in figure 5(*b*). A linear extrapolation shows that the virtual origin is located upstream of the lip at $x_0/D = -0{\cdot}24$, a result consistent with the data of Hussain & Zedan (1978), Husain & Hussain (1979) and Patel (1973) even though other studies (Champagne *et al.* 1976; Batt 1975) found the virtual origin located downstream of the lip for untripped shear layers.

In order to capture some details of the mixing-layer motion, time traces of the linearized $u(t)/U_m$ signal at $x/D \cong 1{\cdot}4$ are presented in figure 5(*c*) for different transverse locations across the mixing layer. (The criteria for selection of this station are discussed later.) Note that the signal on the high-speed side consists of mostly negative

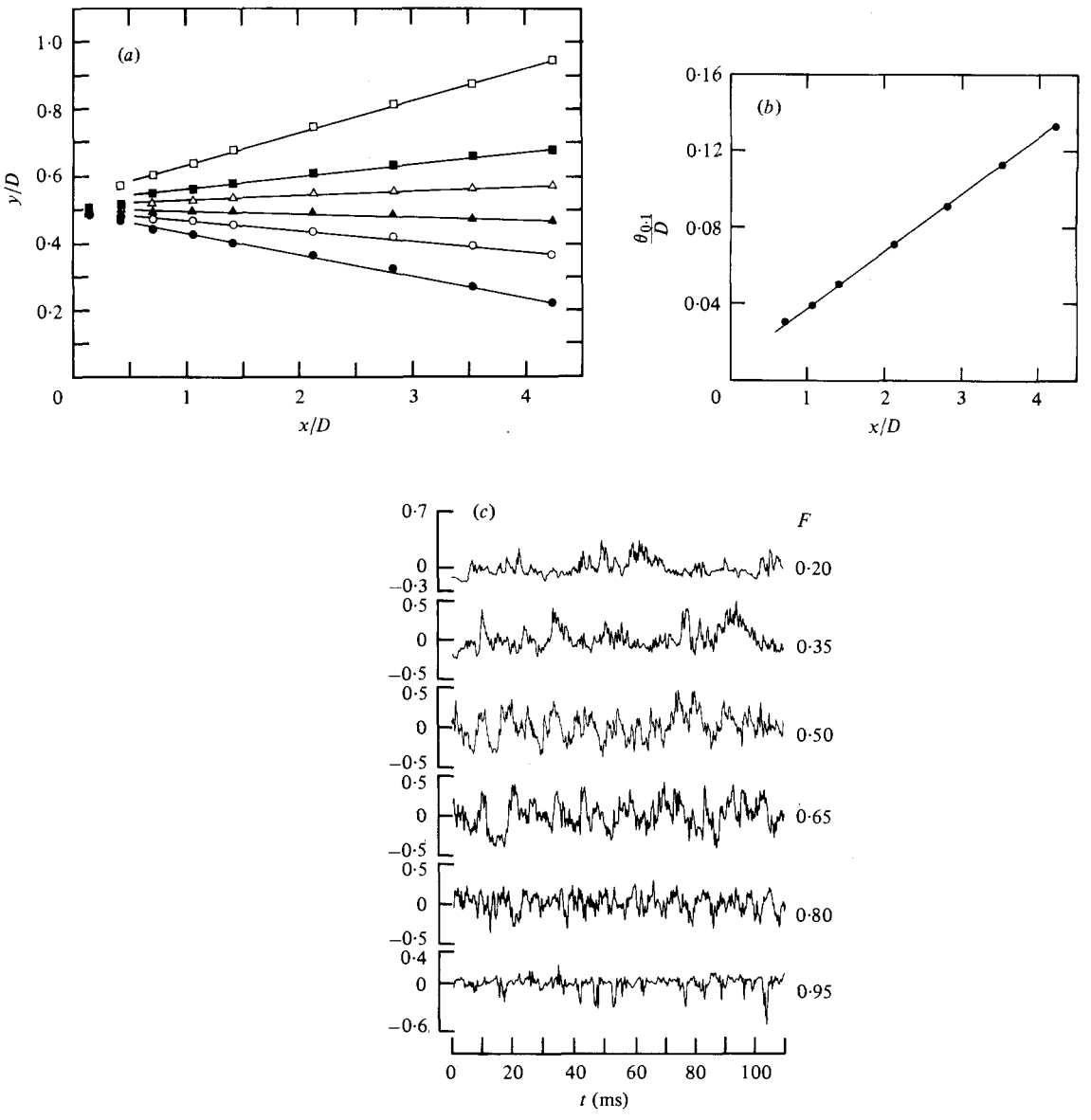

FIGURE 5. (*a*) Lines of constant values of $F = U/U_m$: ●, 0·95; ○, 0·80; ▲, 0·65; △, 0·50; ■, 0·35; □, 0·10. (*b*) Streamwise evolution of $\theta_{0\cdot1}(x)$. (*c*) Time traces of $u(t)$ signal at different transverse locations $F = U/U_m$.

spikes which represent instants of transport of low-speed fluid to the high-speed side. On the low-speed side, the signal consists of positive spikes representing instants of transport of high-speed fluid to the low-speed side. The middle of the shear layer shows no preponderance of positive or negative spikes, suggesting equal probability of outward transport of high-speed fluid and inward transport of low-speed fluid across the middle plane of the layer. Note that the frequency of occurrence of the positive spikes on the low-speed side is considerably lower than the frequency of negative spikes on the high-speed side, an observation which is clearly inconsistent with the notion

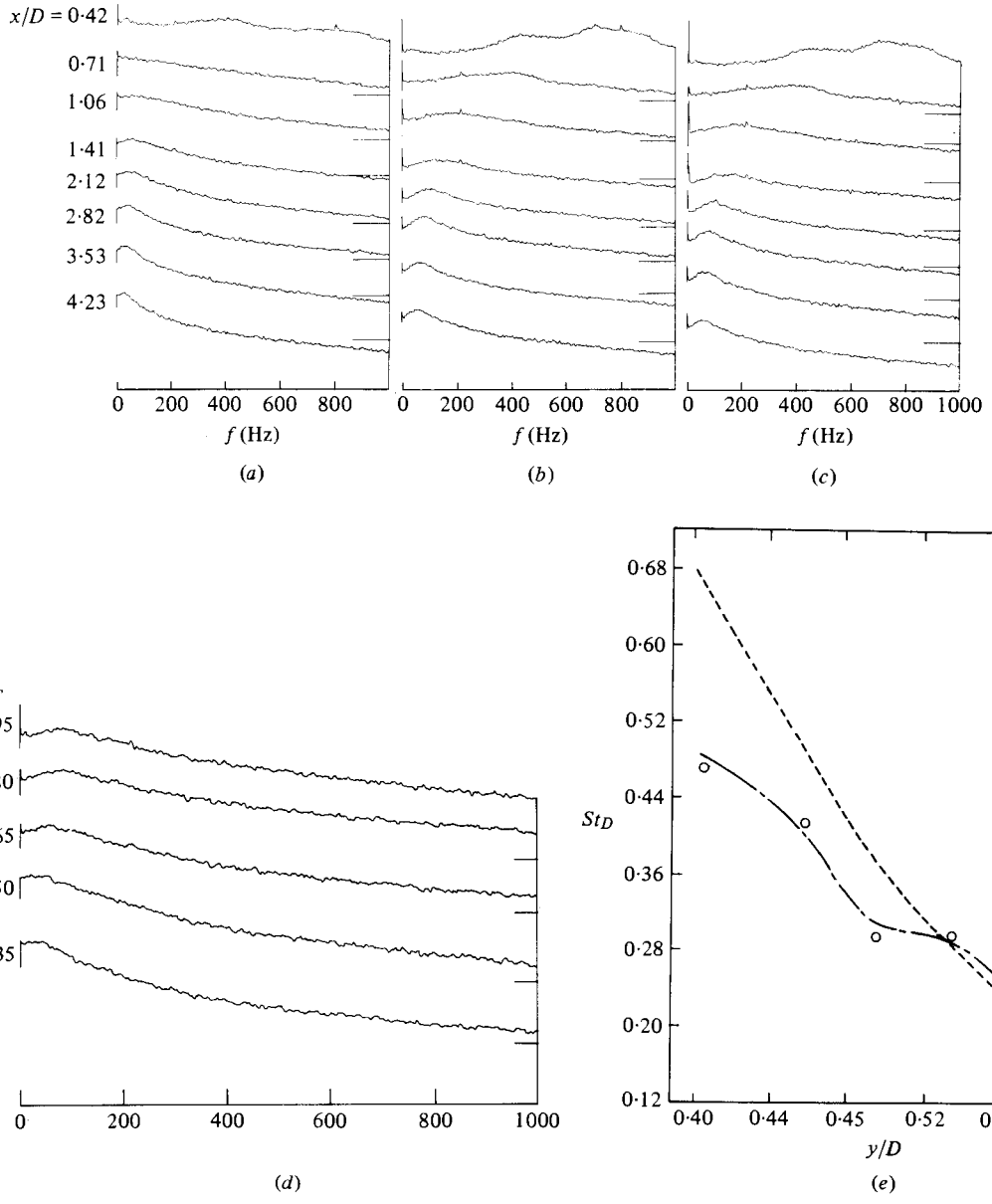

FIGURE 6. (*a*, *b*, *c*) Streamwise evolutions of frequency spectra along $F = 0{\cdot}65$, (*a*) ϕ_u, (*b*) $\phi_{v'}$, (*c*) ϕ_{uv}. (*d*) Radial variation at ϕ_u at $x = 1{\cdot}4D$. (*e*) Radial variation of spectral peak frequency at $x = 1{\cdot}4D$; -----, Lau (1978).

of a single street of large-scale coherent vortical structures constituting the whole mixing layer (Laufer 1974; Lau & Fisher 1975; Bruun 1977; Moore 1977; Yule 1978). Based on our flow-visualization studies, an explanation for the radial variation of the frequency of the spikes is proposed (see later).

The streamwise evolutions of the frequency spectra ϕ_u, ϕ_v and ϕ_{uv} of $u(t)$, $v(t)$ and $uv(t)$ signals along the $F = 0{\cdot}65$ line are shown in figures 6(*a*), (*b*) and (*c*), respectively. The broadband continuous spectra have humps whose frequency values decrease

progressively with increasing x, suggesting progressive growth of large scales with increasing x, presumably through coalescences. The spectra show that the spectral broadening of the fluctuations is essentially complete by $x/D \cong 0{\cdot}70$. Thus, on the basis of congruence of the profiles of U, u', v' and $\overline{uv}$, linear variation of the momentum thickness, and evolution of spectral broadening, the axisymmetric mixing layer can be regarded as having achieved self-preservation at $x/D \cong 0{\cdot}70$. This streamwise distance is considerably longer than the transition distance of $1{\cdot}2 \times 10^5 \nu/U_m$, found by Yule (1978) to be necessary for achievement of full development of the mixing layer.

Figure 6(*d*) shows the radial variation of the u-spectrum ϕ_u across the mixing layer at $x/D \cong 1{\cdot}4$. Choice of this streamwise location as a reference station was dictated by the fact that it is sufficiently upstream from the end of the potential core so that flow can be regarded as a shear layer and sufficiently far downstream from the lip so that the flow can be expected to have achieved self-preservation. Studies in our laboratory together with those of Yule (1978) suggest that vortex pairing activity is essentially complete in a jet by the time this station is reached. It is clear from figure 6(*d*) that the turbulence is broadband across the width of the mixing layer. Taking the frequencies of the spectral peaks in figure 6(*d*), the radial variation of this Strouhal number $St_D = fD/U_m$ is plotted for $x/D \cong 1{\cdot}4$ and compared with the frequency count data of Lau (1978) in figure 6(*e*). Note that this apparently inexplicable large radial variation in St_D prompted Lau to propose the two-street vortex ring model.

3.2. *Characteristics of the mixing layer via flow-visualization*

The details of the mixing-layer motions, vividly captured in the high-speed films, can be appreciated best by viewing the films (at a much slower speed). However, an attempt is made to document limited aspects of these motions in the printed form of the literature as well as convince the reader of the claims made based on these movies by presenting a few carefully aligned picture sequences from the movies. Recognizing the difficulty in conveying the kinematic details of the motions through pictures, the presentation is arranged to include first a graphic tour through the picture sequences, followed by discussions of identified flow events of interest. The resulting inevitable slight redundancy of the discussions as well as of some of the picture sequences included is somewhat intentional on two counts: the events observed are not isolated, and there is significant dispersion in each type of event since no event exactly repeats itself. The extent of this dispersion should guide the reader to make his own judgement on the uncertainty bounds of the observations and claims.

Figures 7(*a*), (*b*) show two sequences of enlarged pictures taken from the high-speed ciné film. These pictures cover the maximum x-range of the shear layer filmed, namely, $0{\cdot}5 \leqslant x/D \leqslant 3{\cdot}5$. As for all the pictures to be presented, the reference lights are shown in the topmost picture of each column sequence. The streamwise position x/D (corrected for parallax) is indicated at the bottom of each column. The direction of the flow is from left to right, and time increases with increasing frame number (marked on the side) from the top to the bottom of the page. The time increment δt between successive frames, which depends on the location of the printed frame sequence with respect to the beginning of the film, has been included in the figure caption. Figure 7(*a*) captures a typical, but infrequently occurring, event of organization of the mixing layer. The initiation of the mixing-layer evolution to the organized state can be followed starting with frame 2, which shows an elongated concentration of

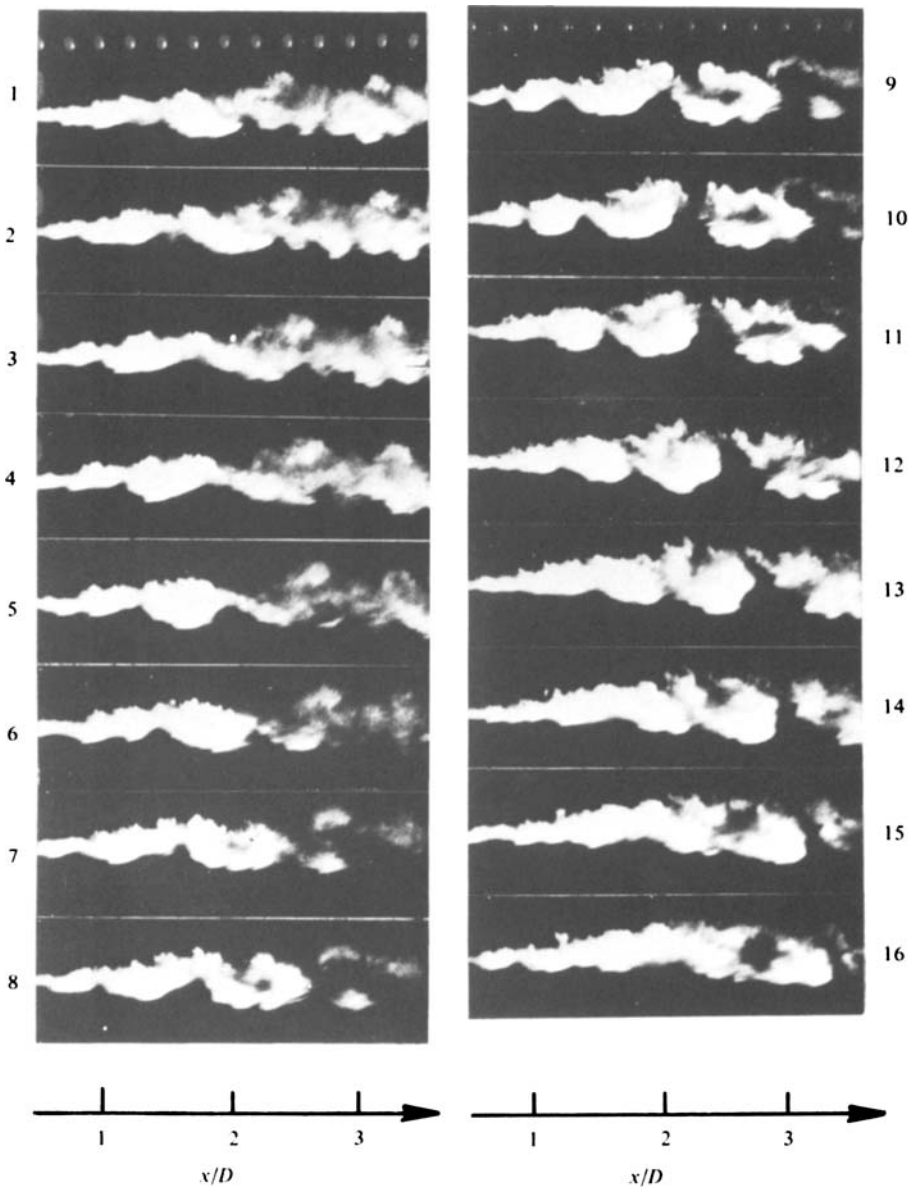

FIGURE 7. Picture sequences for $0{\cdot}5 < x/d < 3{\cdot}5$.
(*a*) $\delta t = 1{\cdot}52$ ms; (*b*) $\delta t = 1{\cdot}43$ ms.

smoke, marking a vortical fluid parcel centred at around $x/D = 1$. By frame 5, this fluid parcel has become somewhat rounded, its width being approximately equal to the local width of the mixing layer; the formation of this structure takes about 4·8 ms. Notice that this newly formed structure survives only a short period of time as the higher-speed inner (lower) portion tears away (frames 7–13) and is swept downstream leaving the slower, outer portion behind. One can track the development of two adjoining large-scale structures at $x/D \simeq 1$ and 1·8 in frame 9, which appear to 'pile up' (frames 12–15) and diffuse into a larger turbulent patch of fluid in frame 16. The

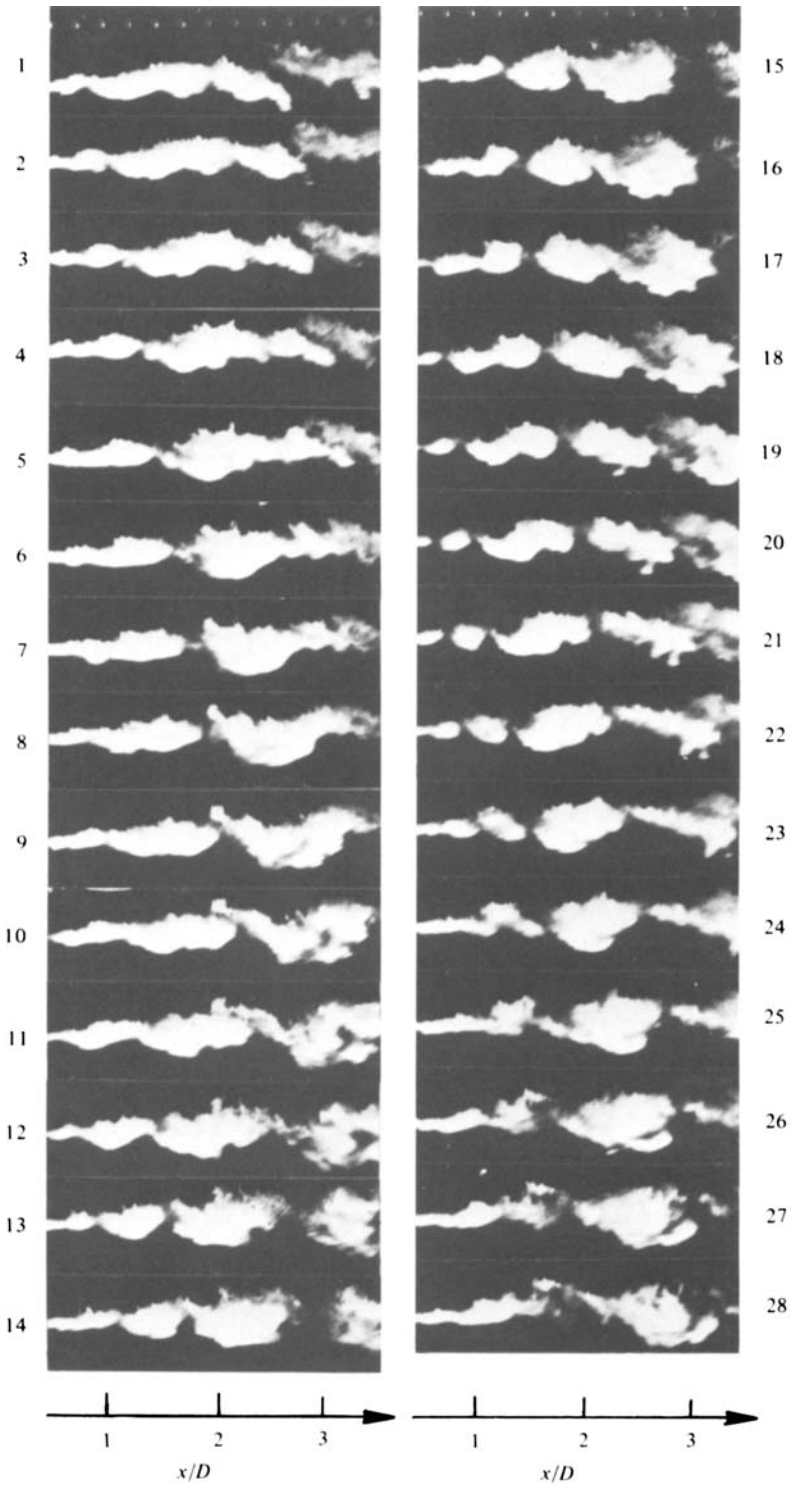

FIGURE 7(*b*). For legend see opposite.

state of organization (or disorganization) in frame 16 looks somewhat similar to that in frame 1.

Figure 7(*b*) shows an example of sustained state of organization of the mixing layer. This sequence captures an event of vortex pairing starting in frame 17, which shows two distinct large-scale vortical structures located at $x/D \cong 1$, and separated by approximately $0{\cdot}5D$. By frame 19 the two structures can be seen to have begun the merger as the trailing structure has started moving under the leading one. If this sectional view is that of a toroidal structure, this movement represents the 'leapfrog' motion between two adjacent structures. From frame 23 on, only the single new combined structure is apparent. Note, however, that, starting from frame 23, an inner portion of this new but apparently 'paired' structure is being torn away from its main body by the high-speed potential core fluid. Thus, the structures themselves are very transient: most large scales which are formed soon get torn apart or undergo decay (see later).

It is also interesting to note the arrested motion of the small smoke-marked fluid element which is ejected into the ambient side of the layer (top centre of frame 8, figure 7*b*) even though it can be identified as a tiny speck in frame 4. Note that this fluid element remains essentially stagnant, i.e. fixed in x, for quite some time (frames 4–14) while the remainder of the visible flow advances downstream. By frame 15 this fluid element can no longer be distinguished. The essentially zero streamwise speed of this fluid element on the low-speed side can be contrasted to the rapid downstream motion of fluid lumps moving along the inner edge of the mixing layer, at speeds comparable to or even higher than U_m. For example, see the small fluid element in frames 19–23 and the lump of fluid in frames 24–28, both on the high-speed side of the mixing layer (see also figure 10*b* which shows the corresponding space–time trajectories of these fluid parcels). Careful examination of the smoke-marked fluid element ejected radially outward (frames 8–14) shows that there is an upstream movement of this element with respect to the laboratory frame, being induced by the mixing-layer large-scale structure motion (discussed later).

Figures 8(*a*), (*b*), and (*c*) show three sequences of picture frames taken from one of the films covering the more limited spatial range $1{\cdot}3 < x/D < 3{\cdot}2$; figure 8(*d*) shows a continuation of the sequence in figure 8(*c*). In these pictures the details of the flow are relatively magnified. The pictures in these sequences capture the events in the lives of some of the more prominent (but infrequently occurring) large-scale structures in the mixing layer. Note that the shapes of the structures in each of the picture sequences are ever changing due to the effect of shear and diffusion. An example of this shape change is provided by the picture sequence of figure 8(*a*) (frames 11–19). In frame 11, the structure on the left-hand side (located at $x/D \cong 1{\cdot}7$) is elongated with its leading edge slightly inclined to the jet axis. With increasing time, this inclination increases. As this rotation takes place, the leading edge of the structure is ejected further out into the low-speed region. Simultaneously, the trailing (higher-speed) part appears to move radially inward as it 'catches up' with (i.e. attains the streamwise position of) the outer part of the structure (frame 16). During this time, the structure broadens in width so that by, say, frame 15 or 16, its radial cross-section is roughly circular. Beyond frame 17, the structure can be seen to begin breaking up.

Figure 8(*b*) shows the formation and evolution of a large-scale structure. This particular formation event appears to be the result of pairing of two structures, one

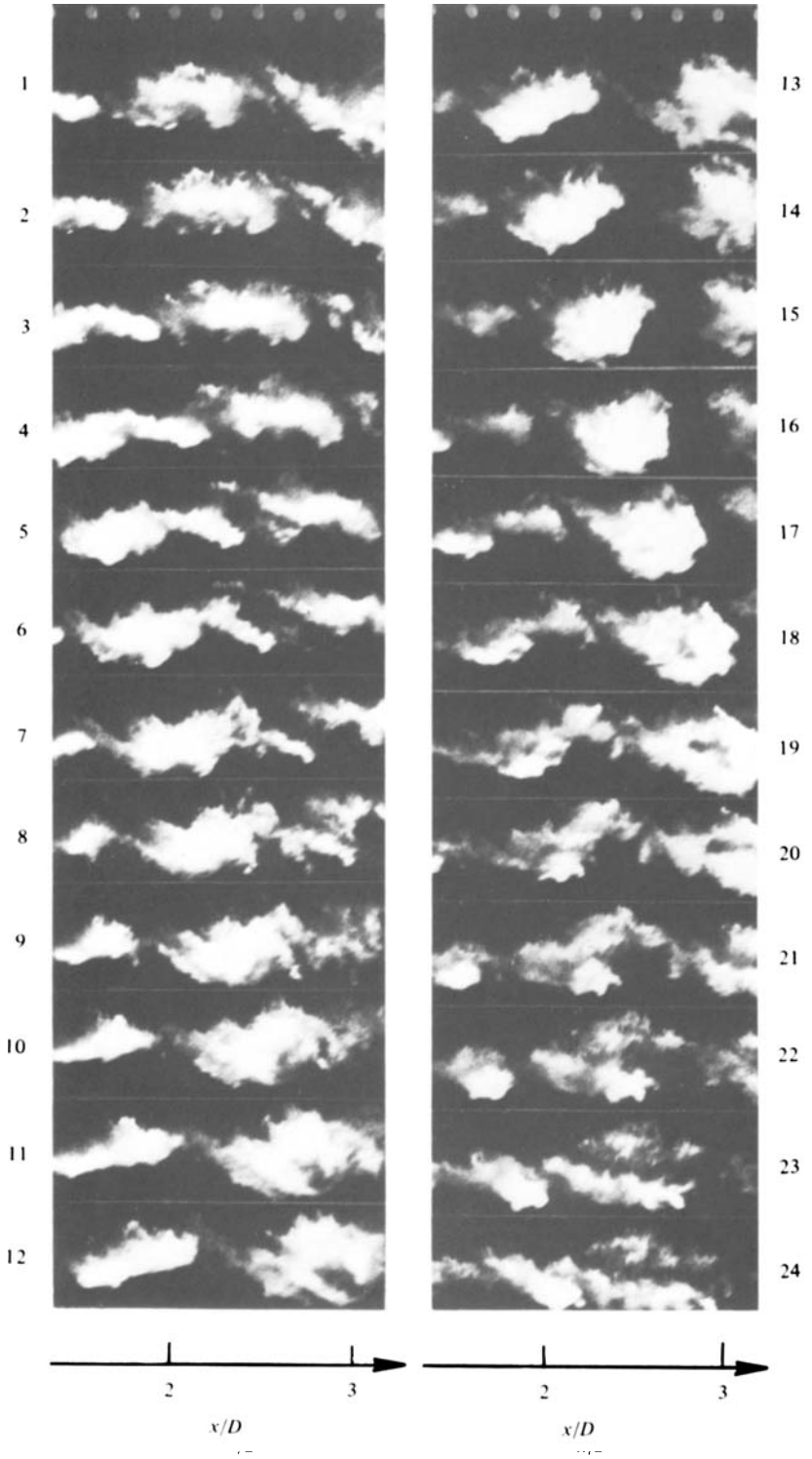

FIGURE 8. Picture sequences for $1{\cdot}3 < x/D < 3{\cdot}2$. (*a*) $\delta t = 0{\cdot}74$ ms; (*b*) $\delta t = 0{\cdot}82$ ms; (*c*, *d*) $\delta t = 0{\cdot}56$ ms.

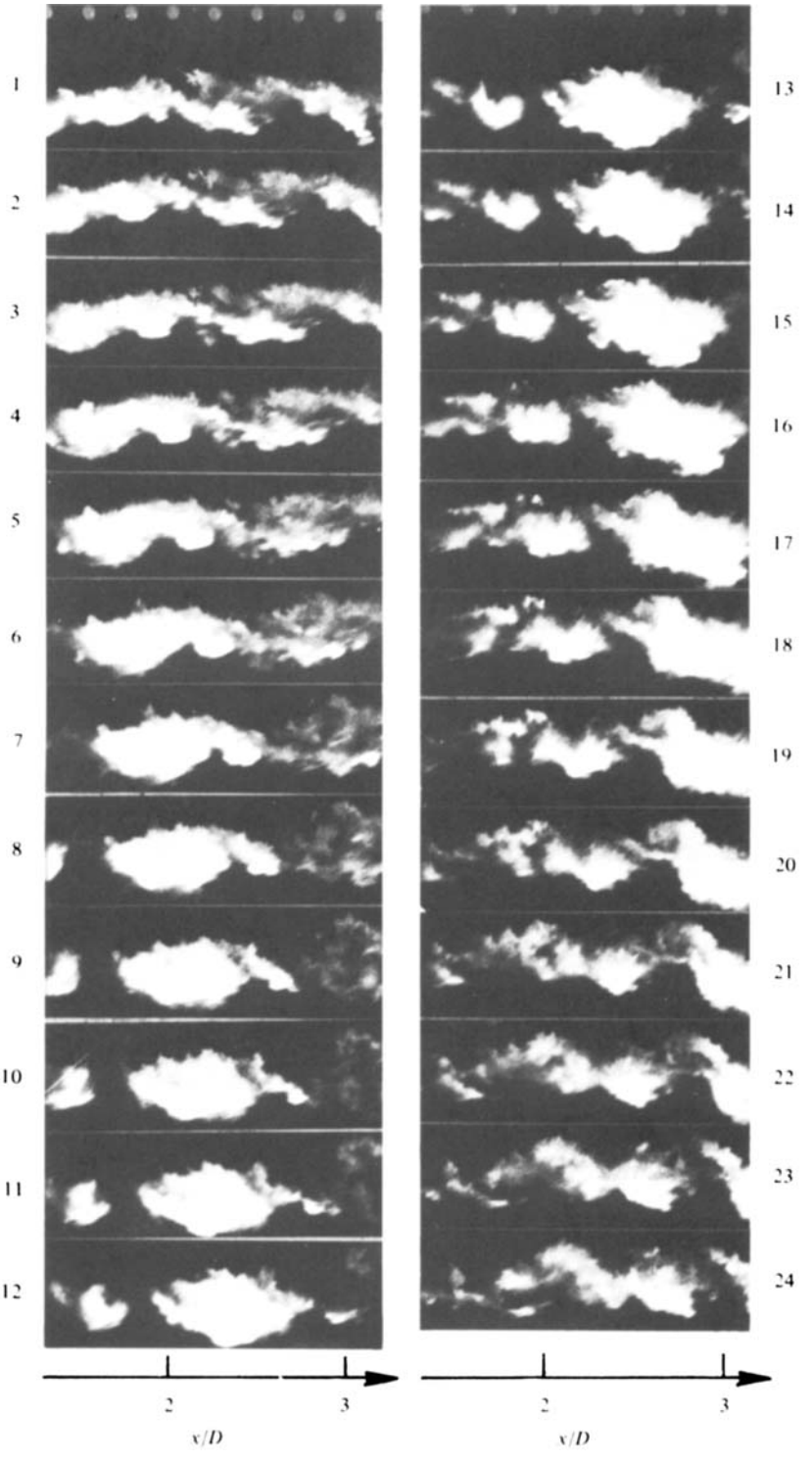

FIGURE 8 (*b*). For legend see page 277.

(the leading structure) centred at $x/D \cong 1{\cdot}7$, and the other (trailing) structure centred at $x/D \cong 1{\cdot}3$ (frame 2). Starting with frame 2, the two structures are seen to merge into a single structure of roughly elliptical cross-section, centred at $x/D \cong 2$ (frame 10). As this structure continues downstream, it is seen to deform continually under the effects of shearing, and by frame 18 it has begun to lose its identity as it moves out of view. It is interesting to note that the smaller-sized structure following the larger merged structure in frame 8 grows in area with time. By frame 22, two such structures can be identified, the upstream one coming into view seemingly via azimuthal motion (frames 13–22).

By use of the timing marks on the films (not visible in the pictures), it is possible to approximate the convection speed of a particular flow event or feature. Note that the speed determined depends upon the particular (large-scale) flow event of interest; for example, the leading and trailing edges of a large-scale structure are observed to move at different speeds. Such differences are easily seen by viewing the picture sequences edgewise.

Figure 8(*c*) shows a good example of such a convection velocity variation between different features of a single large-scale structure. The structure can be followed from frame 1 (where it is centred at $x/D \cong 1{\cdot}5$) through frame 23, at which point it has become quite diffuse as it moves out of the field of view. The convection velocity of the structure leading edge is found to be $0{\cdot}62U_m$ (frames 15–21), whereas for the trailing edge it is $0{\cdot}44U_m$ (frames 15–21). The difference $0{\cdot}18U_m$ between these convection velocities indicate that the back of the structure is receding with respect to its front.

The rationale for the front of a structure to move faster than its back can be found in the fact that the fluid at the front originates from the high-speed side, whereas the fluid at the back originates from the low-speed side; that is, the entrained high-speed fluid is mostly added at the front, while the low-speed, outer fluid is mostly added at the back. Note the depletion of the vortical fluid 'braid' in front of the large-scale structure in frames 16–19. Such depletions are due to migration of the braid fluid to the structure cores under the influence of strain by the adjoining structures and is consistent with hot-wire data taken in our laboratory (Hussain & Zaman 1980) and the theoretical prediction of Corcos & Sherman (1976).

It is interesting to follow the development of the small fluid element shown at the extreme left in frame 7. With increasing time, this element appears to grow rapidly over a relatively short streamwise distance. However, this 'growth' appears to be due more to the circumferential (i.e. azimuthal) movement. Beginning in frame 12, a higher-speed elongated structure can be seen moving under the slower (outer) fluid (frames 12–24). Note the wide difference in the convection velocities of these two parts of the flow; the outer portion remains essentially fixed in x while the inner high-speed fluid convects downstream relative to the outer part. [The fact that different convection velocities are obtained for different parts of the same large-scale structure depending upon the chosen feature of interest points to the need for determining statistical averages; the spectral approach for quantitatively determining convection velocity as a function of wavenumber (Wills 1964, 1970; Clark 1979) provides, for a particular wavenumber (structure spacing), the dominant phase speed at that wavenumber.]

The film sequence in figure 8(*d*) captures the continuation of the rotation and relative 'sliding' effect depicted in figure 8(*c*) (frame 10 in figure 8*d* corresponds to frame 24 in figure 8*c*). The elongated inner structure (say, structure B), which in frame 1 of figure

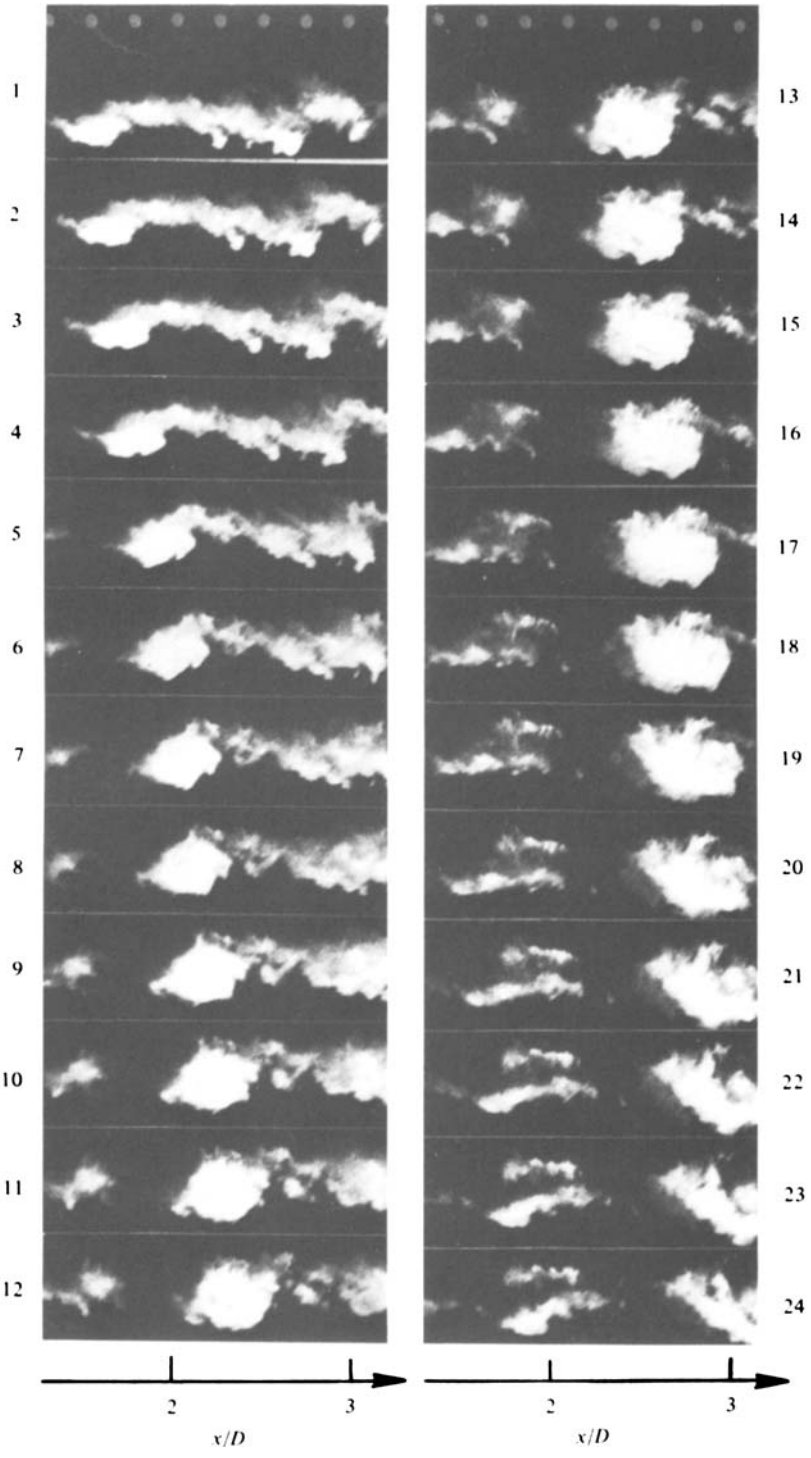

FIGURE 8 (*c*). For legend see page 277.

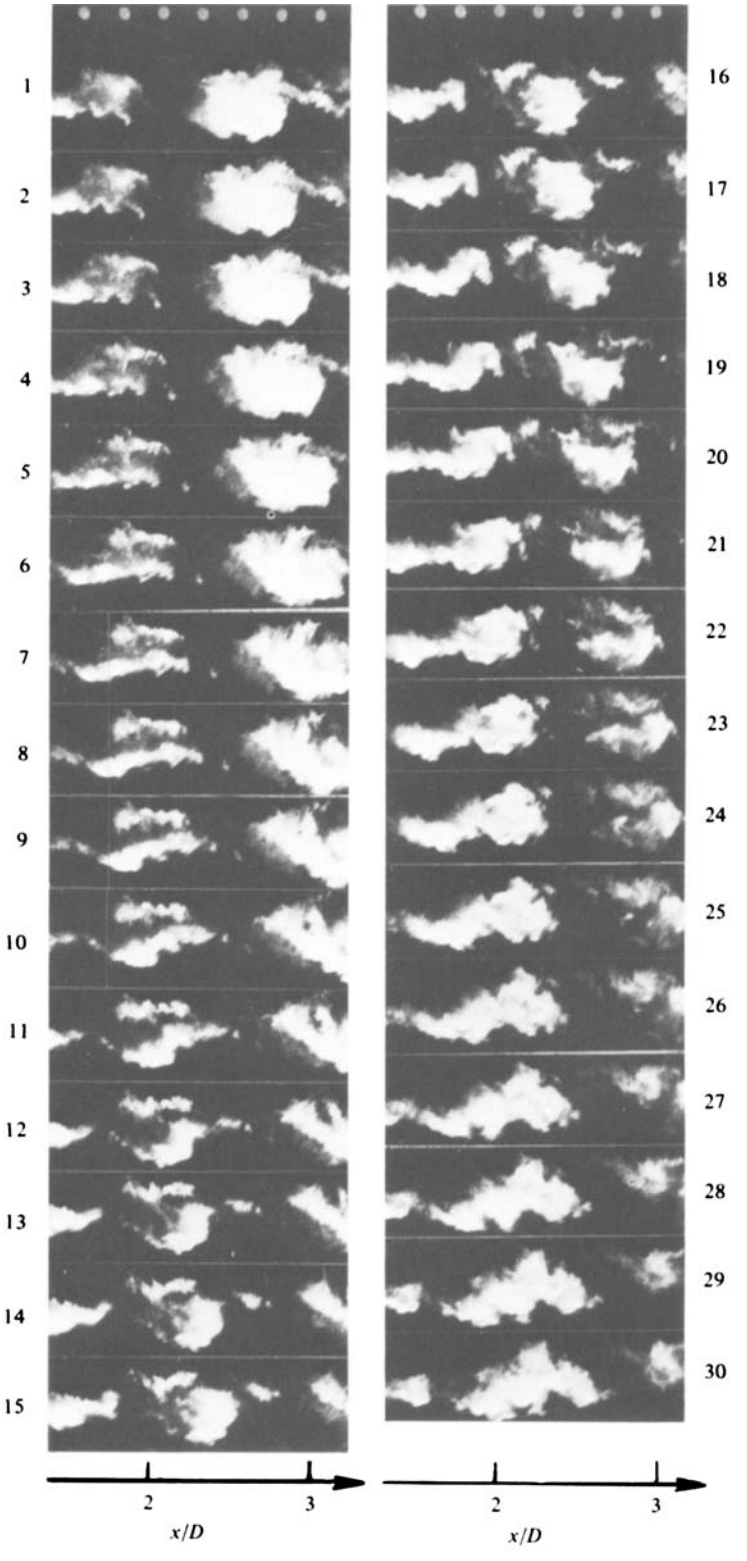

FIGURE 8 (*d*). For legend see page 277.

8(*d*) trails the outer more diffuse structure (say, structure A), can be seen to catch up (roughly in frame 9) and then move ahead of A. This advancing structure B, which began to rotate while still trailing A (frame 4), has rolled into a rounded shape (frame 15) as it continues downstream and merges (frames 19–21) incompletely with a fluid lump which was initially a portion of B itself (see frames 8–13). During this same time, the initially leading low-speed structure A slowly decays while remaining essentially stationary (frames 8–25). Part of A is 'consumed' by B, and the remainder essentially remains stationary on the low-speed side until overtaken by the trailing structure.

The streamwise distances required for both formation and expiration of the large-scale structures are observed to be roughly equivalent to their size. Figures 9(*a*) and (*b*) show the formation and lifespan of two large-scale coherent structures. Figure 9(*a*) shows the formation of a large-scale structure beginning with frame 1. In the first 3–4 frames of this sequence, the portion of the mixing layer which ultimately forms into the large-scale structure (shown say in frame 10) takes on a somewhat 'wavy' appearance. As the faster, trailing fluid overtakes the slower outer fluid, the shape of the structure evolves continuously into the fully formed state shown in frame 10. The streamwise distance taken for this formation is approximately $0{\cdot}5D$. From frame 13 on, the structure begins breakdown and, although still identifiable at the end of the sequence, the structure is very diffuse. The streamwise distance between the point of formation of the structure (say frame 10) to the point where it is essentially diffuse (say frame 24) also corresponds to about $0{\cdot}5D$. Tracking the large-scale structure from frame 10 until frame 24, a clear perception of its motion is apparent; it is clear that the coherent structure has undergone breakdown in the distance from $x = 1{\cdot}5D$ to $2D$. Figure 9(*b*) shows another example of coherent structure formation beginning with frame 2. (The gaps in frames 17 and 18 were produced by accidental scratching of the film during development). By frame 12 the structure is fully formed (located at $x/D \cong 1{\cdot}2$). This formation spans the range $0{\cdot}6 < x/D < 1{\cdot}2$. Note that the organization shown in this sequence is much weaker than that shown in figure 9(*a*). Both the figures 9(*a*) and (*b*) showing two examples of the same flow region with the same initial condition are included so that, in addition to serving as vivid documentation of the mixing-layer coherent structure, these also indicate that there are large dispersions in the nature of organization when it occurs.

The survival distances of the large-scale structures (comparable to their average size) are apparently significantly smaller than those reported for the large-scale structures in a turbulent boundary layer. From space–time correlation measurements of the wall static pressure beneath a turbulent boundary layer, Willmarth & Wooldridge (1962) found the survival lengths of the large scales to be approximately 6λ. In this connection, the coherent structure ('turbulent spot') induced by a spark in an axisymmetric mixing layer (Sokolov *et al.* 1980) and in a plane mixing layer (Kleis & Hussain 1981) has been found to undergo a much more rapid change than that experienced by a similar turbulent spot in a boundary layer (Zilberman *et al.* 1978; Wygnanski 1978, private communication).

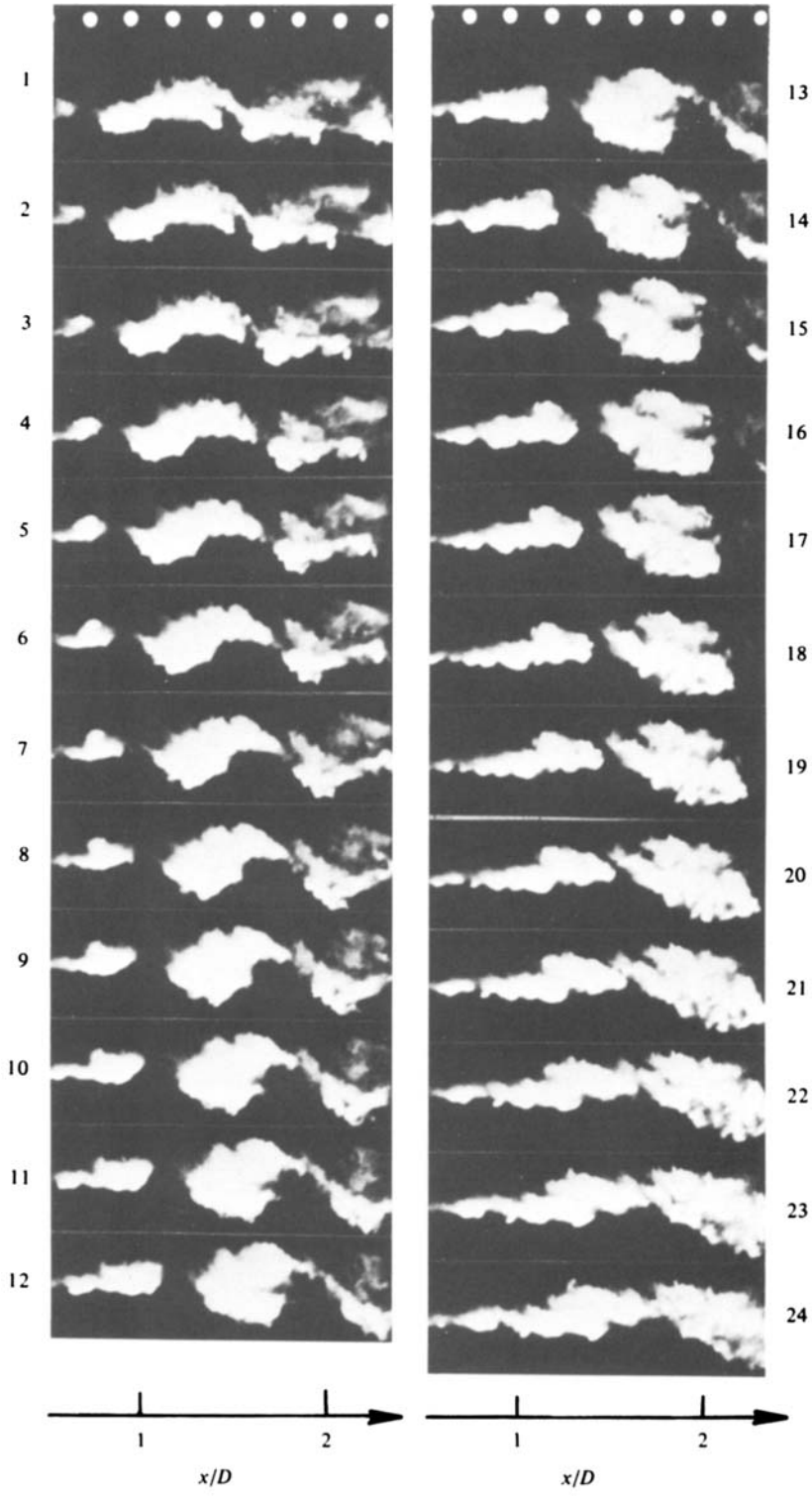

FIGURE 9. Picture sequences for $0{\cdot}5 < x/D < 2{\cdot}4$. (*a*) $\delta t = 0{\cdot}50$ ms; (*b*) $\delta t = 0{\cdot}56$ ms.

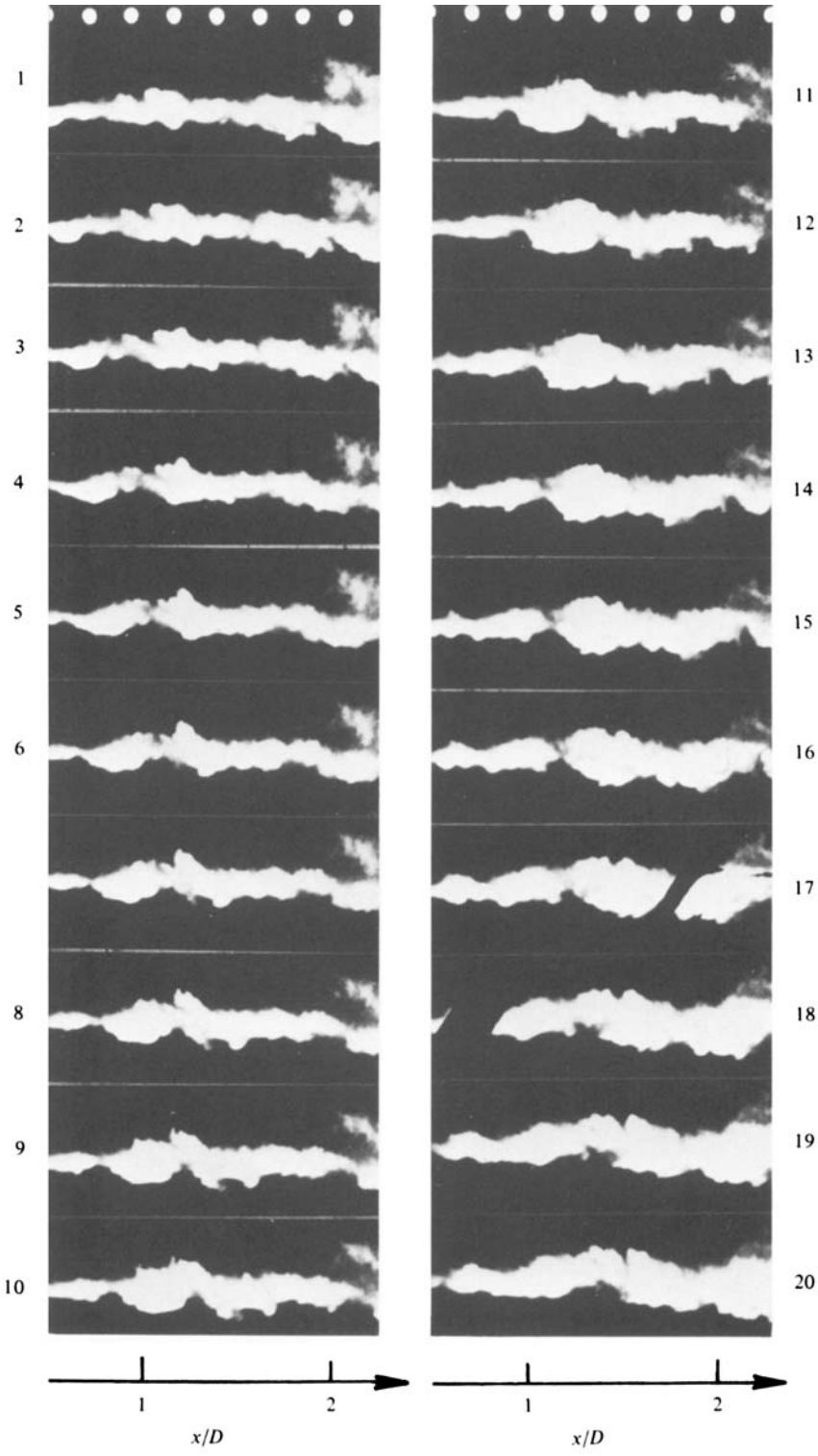

FIGURE 9(*b*). For legend see page 283.

3.3. *Discussion of flow-visualization observations*

To what extent does the initially introduced smoke mark the vortical fluid of the mixing layer? We have visually observed that the smoke is entrained first as a thin laminar sheet downstream from the lip before being rolled up in the initial laminar vortex. Since this vortex subsequently breaks down to turbulence and in the process mixes up the vortical fluid with smoke, it is reasonable to assume that the smoke continues to mark the vortical fluid in the turbulent mixing layer. The molecular diffusion time scale being a few orders of magnitude larger than the advection or turbulent time scale, it is reasonable to assume insignificant the extent of molecular diffusion except smearing of smoke or vorticity boundaries. Thus, the distance between smoke and vorticity boundaries is not likely to be appreciable compared to the large structure sizes, and the smoke boundaries are thus approximately the boundaries of the turbulent shear layer.

The picture sequences presented reveal the structure of the axisymmetric mixing layer at the highest Reynolds number known to have been investigated in detail through flow-visualization. As such, these pictures provide some interesting details of the highly debated and yet-to-be-understood state of the flow structure of a mixing layer. Yule (1978) claims that the low-speed side of the mixing layer is diffuse and jagged, while the high-speed boundary is sharp and smoothly convoluted such that individual large-scale coherent structures of the layer can be easily discerned on the high-speed side. Our films capturing instantaneous contours of the structures, say figure 8(*c*), (*d*) and 9(*a*), (*b*) do not suggest such obvious difference between the two boundaries.

Examination at slow speed of the high-speed flow-visualization cine films suggest that unlike the flow at lower Reynolds numbers, the mixing layer is mostly in a state of disorganization without any distinct large-scale coherent structures. Some perception of the state of disorganization can be obtained from frames 1, 16 of figure 7(*a*) and frames 1, 20 of figure 9(*b*). Thus, for the sake of brevity, a separate picture sequence of the mixing layer showing its disorganized state is not included. No attempt was made in this study to quantify the extent of disorganization of the layer.

The flow-visualization films also show that the mixing layer is organized into large-scale vortical structures only infrequently. These structures are seen to be short-lived, their lack of longevity being contributed to by four types of events: (i) tearing, (ii) pairing (complete as well as fractional), (iii) 'slippage' of one structure under another, and (iv) breakdown (or decay). Although not as clear as we have observed in the same mixing layer at lower flow speeds (pictures not presented), or as seen in other low-speed flows (Winant & Browand 1974; Zaman & Hussain 1980), complete pairing has been found to occur occasionally (see, for example, frames 17–24 in figure 7*b*).

More often than not, however, pairing is partial in nature, i.e. not all of the fluid associated with the two merging structures completely coalesce: one structure captures a part of an adjoining structure. Occasionally there is 'fractional pairing', i.e. merger between parts torn from different initial coherent structures. Tearing may occur during the final stages of a pairing event (see, for example, frames 24–28 of figure 7*b*). The single fluid lump located at $x/D \cong 1$ (frame 21 of figure 7*b*) is being torn apart by the adjoining structures on either side (frames 21–25); its two parts then separately merge with the adjoining structures. Figure 8(*b*) shows an example of partial pairing (starting from frame 2) of two large-scale structures in the sense that part of the leading structure

does not merge. There are also occasions (frames 7–14 of figure 7*b*) of one structure capturing merely a part of an adjacent structure (the outer, slower part of the structure in frames 7–14 of figure 7*b*) without substantially affecting the remainder. The formation of a large-scale structure also results from complete merger (frames 1–10 of figure 9*a*) even though it can occur as a growth of a rolled-up structure (frames 2–12 of figure 9*b*). Structures which do not happen to be torn apart are found to increase in size, deform and become progressively diffuse (frames 7–24 of figure 9*a*, frames 4–24 of figure 8*c*, frames 7–12 of figure 7*b*) or stretched out (frames 15–23 of figure 7*b*) under the action of shear.

Some features of the smoke boundaries can be used to estimate rotation rates of the large-scale structures. For example, the linear part of the right-hand boundary of the structure at $x/D \cong 2{\cdot}3$ (frame 15) in figure 8(*a*) shows a counter-clockwise rotation of about 90° between frames 14 and 18. Similarly, the structure at $x/D \cong 2$ (frame 5) in figure 8(*c*) undergoes a rotation of about 60° between frames 5 and 9. The leading edge of the same structure show that it later rotates by about 45° between frames 2–5 of figure 8(*d*). From these rotation angles, the average time for one revolution is found to be about 12 ms. Taking the structure convection velocity to be $0{\cdot}6U_m$, the survival time of a structure is also found to be approximately equal to one 'turnover' time. Note that either of these two periods is about 5 times the local shear layer time scale δ_ω/U_m, where δ_ω is the local thickness of the layer.

The films reveal three-dimensionality of the structure motions as evidenced by the arrrival or disappearance of smoke-laden fluid parcels from the illuminated plane, at a rate too fast to be attributable to diffusion. Note, for example, the disappearance of smoke on the right-hand side between frames 3–7 of figure 7(*a*), frames 3–9 of figure 8(*b*) and frames 2–12 of figure 9(*b*). Note also the appearance of smoke on the left-hand side between frames 13–24 of figure 8(*b*), frames 6–22 of figure 8(*c*), frames 7–12 or 14–19 of figure 8(*a*) and frames 7–12 of figure 9(*a*). These three-dimensional components of the flow may be related to an azimuthally dependent large-scale structure. From phase-locked azimuthal correlation, Hussain & Zaman (1980) inferred an azimuthally lobed large-scale structure in the mixing layer of an excited circular jet. Such modes have also been visually observed (Browand & Laufer 1975; Davies & Baxter 1978; Yule 1978) as well as analytically predicted (Widnall 1975; Saffman 1978).

Note that the sensitivity of the thin light-sheet illumination to the azimuthal motion is also a constraint of the flow-visualization technique employed because one can argue that the apparent streamwise variations of the structures may be partly a result of the azimuthal motion of the structures. We have been well aware of this constraint, recognizing that there is no completely satisfactory answer to this question. Various other visualization methods and lighting techniques were experimented with and, in spite of this constraint, the thin sheet illumination technique was still preferable to all others available. Note that the streamwise changes of the cross-sectional areas of identified isolated structures are not indeed very large. Thus there is little question that events like pairing, tearing, slippage, breakdown, etc. are inferred from evolutions of the same smoke-marked fluid parcels. Examination of the film sequences clearly eliminates the possibility that these apparent events can be artefacts of the illumination technique.

Probably the most striking contribution of the flow visualization film sequences is a clear physical perception of the convection velocity, as well as the recognition of

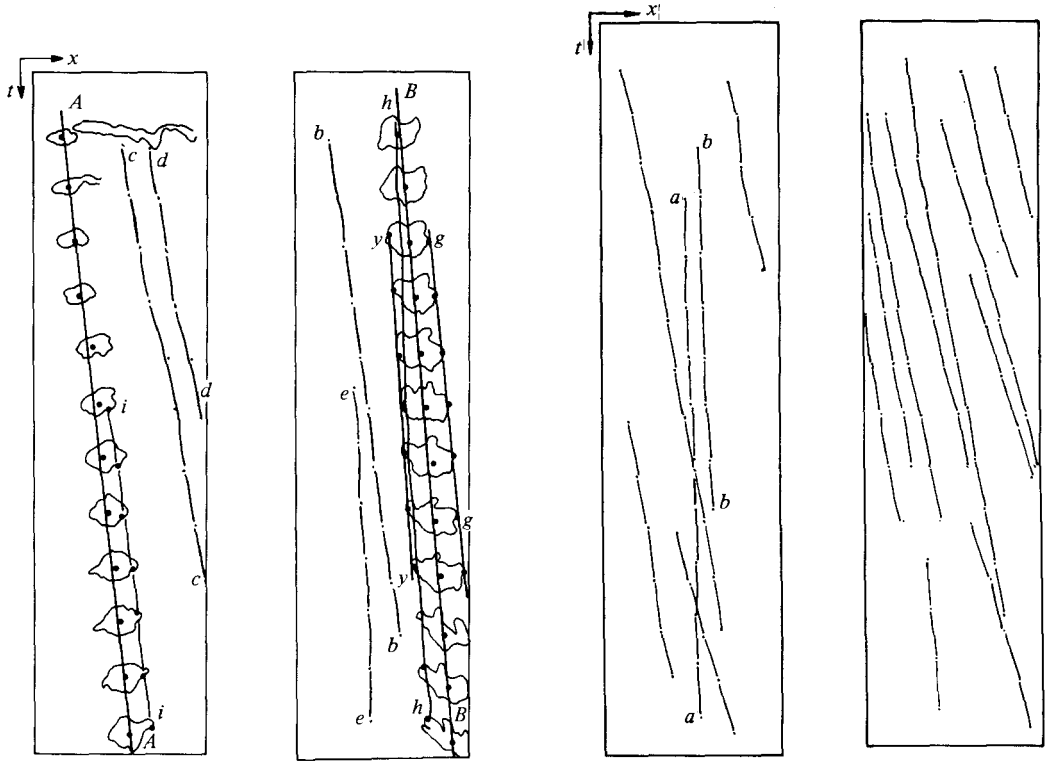

FIGURE 10. Space–time trajectories of fluid elements in picture sequences corresponding to (*a*) figure 8(*c*); (*b*) figure 7(*b*); (*c*) figure 8(*b*); (*d*) figure 8(*d*).

difficulties in its measurement. Since specific structures have been identified in successive frames, the time differences between frames and translation distances in x of the structures should provide this convection velocity.

When viewed edgewise, the slopes of lines connecting identified structure centroids in a sequence provide a direct measure of the convection velocity (see, for example, figures 8*c*, *d*, 9*a*). However, the convection velocity is a distinct function of the specific feature chosen, as well as of the radial position, since the same fluid element moves across the layer while advecting downstream. Furthermore, a structure convection velocity is meaningful only over a short distance or time over which the structure persists in some characteristic shape.

Figure 10(*a*) shows lines (*AA* and *BB*) connecting the approximate x-locations through which the centroid of the cross-section of the evolving large-scale structure shown in figure 8(*c*) passes. From the essential linearity of these two lines, one can infer a constant convection velocity of the coherent structure. Since the structure increases in size as it progresses downstream, its leading edge moves faster than its trailing edge, as can be seen by comparing the slopes of lines *g*–*g* and *y*–*y*. The other lines, for example *c*–*c*, *d*–*d*, track the space–time trajectories of individual smoke-marked fluid elements which can be identified through comparison of figure 10(*a*) with figure 8(*c*).

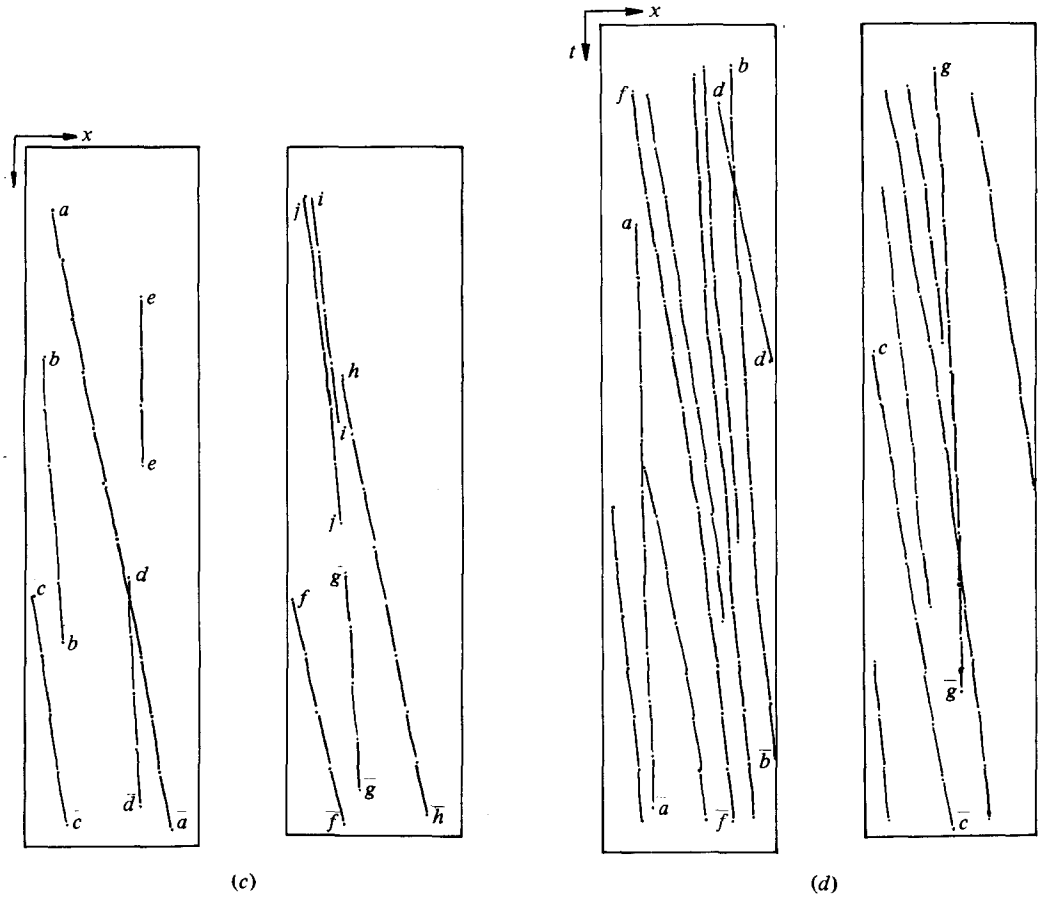

FIGURE 10(c, d). For legend see page 287.

Figures 10(*b*)–(*d*) show space–time trajectories of specific flow features, i.e. fluid elements, in figures 7(*b*), 8(*b*), (*d*), respectively.

From these space–time trajectories in the (x, t) plane, the convection velocities $U_c = dx/dt$ of identified flow features, viz. either of a coherent structure as a whole or individual fluid elements identified by smoke, can be determined. For example, the average slope of the lines *A*–*A* or *B*–*B* in figure 10(*a*) gives the convection velocity of $0{\cdot}6U_m$ for the large-scale coherent structure captured in the picture sequence in figure 8(*c*). This value agrees well with the dominant convection velocity U_d towards the core side of the mixing layer, determined from the wavenumber–celerity spectrum data (Clark 1979; Clark & Hussain 1980). This spectrum was obtained from double-Fourier transformation of the longitudinal velocity space–time correlation between two hot-wires separated in the streamwise direction. The convection velocity of $0{\cdot}72U_m$ found by Yule (1978) is considerably higher than our value, presumably because Yule's measurements were taken in the high-speed half of the mixing-layer width. The convection velocity of a spark-induced coherent structure 'spot' in an axisymmetric mixing layer was found to be about $0{\cdot}68U_m$ (Hussain *et al.* 1980). However, our value of $0{\cdot}6U_m$ is in close agreement with the convection velocities of natural

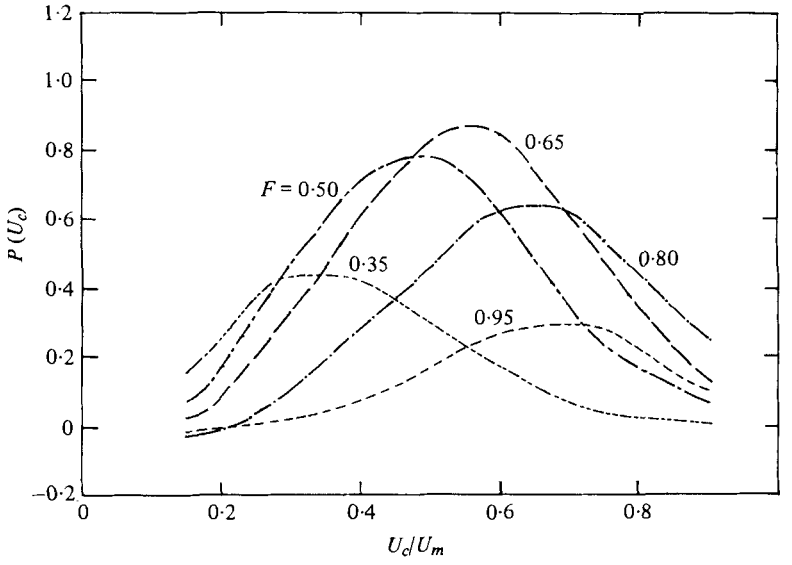

FIGURE 11. Probability density of convection velocity U_c at different locations across the width of the shear layer at $x = 1{\cdot}4D$.

structures in the axisymmetric mixing layer measured by Ko & Davies (1971), Lau *et al.* (1972), Bradshaw *et al.* (1964), and Petersen (1978). The convection velocity profile across the mixing layer can also be determined in the above-mentioned way, except that an identified fluid element does not always remain in the same relative transverse location (see figures 7–9 and, especially, line *b*–*b* in figure 10*d*). The slopes of the space–time trajectories in figure 10 show a large dispersion in the convection velocity starting with essentially zero velocity on the low-speed side of the mixing layer to progressively larger values towards the higher-speed side. Lines *d*–*d* in figure 10(*a*) and line *d*–*d* in figure 10(*d*) represent convection of marked fluid elements on the high-speed side of the mixing layer. Convection velocities determined from these space–time trajectories (and others not included), however, range from $1{\cdot}06U_m$ to $1{\cdot}14U_m$. These high values can be explained partly by the fact that these identifiable fluid points are rotating counterclockwise with respect to the centres of structures in which they are embedded while the structures themselves are being translated downstream. Thus, while structures typically travel at $0{\cdot}6U_m$, individual fluid elements can advect downstream at speeds in excess of the local maximum mean velocity U_m. The wavenumber–celerity spectrum data also show that the convection velocity can exceed the local mean velocity everywhere in the shear layer, as to be expected.

Figure 11 shows the probability density of the convection velocity $P(U_c)$ at different transverse locations characterized by $F = U/U_m$ in the mixing layer; for measurement details, see Clark (1979). Note the large dispersion in the convection velocity at each F; if the mixing layer is predominantly well organized, such large dispersion in U_c would not occur. For example, at $F = 0{\cdot}65$, convection velocity ranges between $0{\cdot}15U_m$ and $0{\cdot}95U_m$. On the low-speed side, the convection velocity is comparatively more frequently low, seldom exceeding $0{\cdot}75U_m$; on the high-speed side, it is comparatively more frequently high, seldom falling below $0{\cdot}4U_m$. Consequently, low-speed fluid transported to the high-speed side does not retain its original momentum but picks up speed

as it is being transported. Similarly, a high-speed fluid element is considerably slowed down while being transported to the low-speed side. Recognizing that figure 11 merely presents time-average data, we still find it to be quite representative of the average trend inferred from the ciné films. Consider, for example, the $P(U_c)$ curve for the middle of the mixing layer, i.e. $F = 0{\cdot}5$. The probability of the fluid element in the middle of the layer to have a convection velocity U_c higher than $0{\cdot}5U_m$ is about equal to the probability of U_c being lower than $0{\cdot}5U_m$, since fluid particles in the middle originate from either side of the mixing layer. That is why $P(U_c)$ is essentially symmetric at $F = 0{\cdot}5$, while on either side of the layer, $P(U_c)$ is skewed towards the local mean velocity. If the curves are extended towards the high-speed end, note that $P(U_c)$ data show U_c exceeding U_m for $F = 0{\cdot}80$ and $0{\cdot}95$. Note that the probability of U_c exceeding U_m is higher at $F = 0{\cdot}80$ than at $F = 0{\cdot}95$. This apparently perplexing data can be reconciled by the fact that at $F = 0{\cdot}95$ the fluid elements are mostly core potential fluid while at $F = 0{\cdot}80$ these are mostly embedded in the mixing-layer vortical structures and thus more subjected to additional (apparent) advection due to rotation of the coherent large-scale structures.

Occasionally, some parts of a coherent parcel of fluid are ejected sufficiently far into the low-speed region that this fluid temporarily separates from the mixing layer. Lines *a–a* and *b–b* in figure 10(*b*), lines *d–d* and *e–e* in figure 10(*c*), and line *a–a* in figure 10(*d*) represent the event of mixing-layer fluid stagnating after being ejected outward. In some cases, such fluid can be observed to undergo surges of upstream velocity (for example, the bottom of line *a–a* in figure 10*b*) as structures of sufficiently large circulation pass by. The occasional large spikes observed in the signal traces of a cold-wire/hot-wire probe pair positioned in the outer region of a free shear flow in experiments conducted in our laboratory (Hussain & Zaman 1980; Antonia *et al.* 1980) can be attributed to such instants of flow reversal since at these instants the upstream cold-wire lies in the heated wake of the downstream hot-wire. These instants of upstream flow in the laboratory frame on the low-speed sides of jets discharging into stagnant environments (also observed by Chevray & Tutu (1978) and Yule (1978)) indicate an inherent inaccuracy of hot-wire measurement due to signal rectification, for which no satisfactory correction sheme appears feasible because these instants of flow reversal occur both in turbulent and in non-turbulent regions. This is one example where laser-Doppler anemometry enjoys a decided advantage because of its ability to detect and measure flow reversal.

4. The mixing-layer model and concluding remarks

Based on the flow-visualization results presented thus far, several comments can be made concerning the physical model of the axisymmetric mixing layer. The models proposed by Lau *et al.* (1972), Lau & Fisher (1975), and Lau (1978) as well as suggested by Brown & Roshko (1974), Laufer (1974), and Browand & Laufer (1975) would seem to imply that the large-scale structures in the axisymmetric mixing layer are much more organized and prevalent than the results of the present (flow-visualization and hot-wire) study indicate.

Lau & Fisher proposed that the flow field is composed of an axial train of toroidal vortex rings which span the width of the layer and are spaced approximately $1{\cdot}25D$ apart. This simplistic model of Lau & Fisher could not, however, account for some

striking differences observed between the structures on the inner, high-speed side and the outer, low-speed side. More specifically, Lau & Fisher could not reconcile the large radial variation of the structure passage frequency as depicted by large positive and negative spikes in the hot-wire traces (figure 5*c*). Furthermore, the convection velocity determined by using an eduction technique triggered on the positive spikes of the u signal was found to depend upon the radial position in the mixing layer. However, when the negative spikes were used as the trigger event, a nearly constant value of convection velocity was found across the mixing region. Based upon these data, Lau & Fisher (1975) suggested that a separate component of vortices may exist in the outer region of the mixing layer. Later, Bruun (1977) found that coherent structures educed on the basis of positive spikes in the u signal differed from those educed by triggering on negative spikes.

On the basis of the large radial frequency variation (about threefold) across the shear layer (figure 6*e*) and extensive correlation and eduction data, Lau (1978) has proposed a revised 'two-street vortex' model of the axisymmetric mixing layer: the 'main' street, discussed earlier by Lau & Fisher, travels on the inner side of the mixing region along a path which converges on the jet axis at around $x/D = 8$, and the 'branch' street which travels at a lower velocity on the outer edge of the mixing region and gradually radiates away from the jet axis as the street travels downstream. Lau also claims that the vortices of the two streets are toroidal in shape.

High-speed flow-visualization movies capturing the instantaneous smoke-marked fluid contours show that the high-Reynolds-number mixing layer is typically in a state of disorganization and is in intense three-dimensional motion. The layer is occasionally and intermittently organized into distinct large-scale coherent vortical structures, but both the duration of organization and the survival distances of these structures are small. (The survival distance is about the size of the structure and the survival time is about one 'turnover' time.) These observations contradict the suggestions based on recent low-Reynolds-number mixing-layer studies that the turbulent mixing layer, and even possibly all turbulent free shear flows, are dominated by quasi-deterministic large-scale coherent structures. We are not necessarily in total agreement with Chandrsuda *et al.* (1978) who claim that the mixing-layer structure is three-dimensional but probably well organized, nor with Yule (1978) who claims that the axisymmetric turbulent mixing layer, though three-dimensional, is disorganized on the low-speed side but well organized on the high-speed side. Neither three-dimensionality nor helicity of a coherent structure (Chandrsuda *et al.* 1978), if present, would produce a predominantly diffuse sectional view of the mixing layer.

The flow-visualization films show no evidence of the two-street toroidal vortex ring structure proposed by Lau (1978) and Lau & Fisher (1975) and suggest the Lau model to be rather optimistic, even quite unrealistic. Not only that two streets are not observed at all, but there is even no evidence of sustained organization. There are additional reasons for questioning the validity of the Lau model. The naturally occurring toroidal vortex ring structure near the lip of an untripped jet undergoes breakdown through the development of azimuthally lobed structures (Davies & Baxter 1977; Yule 1978); the development of these azimuthal instability modes have also been analytically predicted (Widnall 1975; Saffman 1978). Azimuthal correlation measurements by Hussain & Zaman (1980) show that the toroidal structure in the near field of a circular jet is destroyed before the end of the potential core. Their measurements,

phase-locked to the initial coherent structure, also show that, even when the initiation of the toroidal vortex rings near the lip is organized through controlled axisymmetric excitation, this organization disappears at the end of the potential core. From Yule's (1978) results showing that correlation between u signals from two diametrically opposite points in the mixing layer decreases earlier in x with increasing Re, it would seem that the mixing layer should progressively become disorganized with increasing Reynolds number.

It thus appears that a simple model for the high-Reynolds-number mixing layer is not likely to be successful. Our observations suggest that, while coherent structures are inherent to all turbulent shear flows, their characteristics at high Reynolds numbers cannot be inferred from low-Reynolds-number observations. At high Reynolds numbers, they appear to be less frequent and more complex than suggested before. Does this mean that the correlation coefficient as a function of azimuthal angle decreases with increasing Reynolds numbers? Since we do not have any basis to doubt the principle of Reynolds-number similarity, one possible way to reconcile this would be to suggest that at higher Reynolds numbers, even though the coherent structures occur less frequently, these are likely to be more dominant. A recent study in our laboratory indeed suggests that, with increasing Reynolds numbers, the preferred-mode coherent structure of an axisymmetric mixing layer is more rounded in cross-section and is responsible for production of larger coherent Reynolds stress.

This paper has addressed primarily the nature of organization, even though organized structures appeared to form infrequently, without attempting to quantify the extent of organization or disorganization of the mixing layer. Such quantification is by no means straightforward as it will require coherent structure detection schemes involving sophisticated conditional sampling techniques and will be difficult owing to the large dispersion in the structure characteristics from realization to realization. [The naturally occurring coherent structures in axisymmetric and plane mixing layers and in the far fields of axisymmetric and plane jets are being studied in our laboratory through digital analysis of signals from a rake of sixteen hot-wires.]

Even though use of a thin sheet of light suffers from the constraint that azimuthal motion can confuse the extent of evolutionary changes of structures, it has been argued that events like pairing, tearing, slippage, etc. can be inferred unambiguously. Perhaps simultaneous illumination of two orthogonal planes may help quantify the azimuthal motion and its influence on the apparent structure evolution.

The ejection of the vortical mixing-layer fluid to the ambient appears quite prevalent and is an integral part of the low-speed side jet mixing, which is typically regarded as being only due to entrainment of the ambient fluid.

Tearing, sliding without merger, and fractional and partial pairings of the mixing-layer coherent structures appear to be quite prevalent; pairing is typically of the fractional or partial type, rather that the complete type as is widely believed.

It is proposed that tearing, 'slippage' without merger and fractional and partial pairings are responsible for the observed large radial variation of the structure passage frequency across the width of the mixing layer. This would also explain why the coherent structures educed by Bruun (1977) depended on whether the positive or negative spikes of the u-signal were used as trigger and why Yule's (1978) conditional sampling measurements triggered on negative peaks of u-signals produced no clear coherent structure towards the outer side of the mixing layer.

This research was funded by the National Science Foundation under grant ENG 75-15226. The authors are grateful to Mr Z. D. Husain for his help with the computer-controlled hot-wire data acquisition, and to Dr S. J. Kleis, Dr L. S. G. Kovasznay and Dr K. B. M. Q. Zaman for careful reviews of the manuscript and extensive discussions on the data.

REFERENCES

ANTONIA, R. A., CHAMBERS, A. J & HUSSAIN, A. K. M. F. 1980 *Phys. Fluids* **23**, 871.

BATT, R. G. 1975 *A.I.A.A.J.* **13**, 245.

BATT, R. G. 1978 *J. Fluid Mech.* **82**, 53.

BRADSHAW, P. 1966 *J. Fluid Mech.* **26**, 225.

BRADSHAW, P., FERISS, D. H. & JOHNSON, R. F. 1964 *J. Fluid Mech.* **19**, 591.

BRADSHAW, P. 1977 *J. Fluid Mech.* **80**, 795.

BROWAND, F. K. & LAUFER, J. 1975 *Turb. in Liquids* **4**, 333. Univ. of Missouri-Rolla.

BROWN, G. L. & ROSHKO, A. 1974 *J. Fluid Mech.* **64**, 775.

BRUUN, H. H. 1977 *J. Fluid Mech.* **84**, 641.

CHAMPAGNE, F. H., PAO, Y. H. & WYGNANSKI, I. 1976 *J. Fluid Mech.* **74**, 209.

CHANDRSUDA, C., MEHTA, R. D., WEIR, A. D. & BRADSHAW, P. 1978 *J. Fluid Mech.* **85**, 693.

CHEVRAY, R. & TUTU, N. K. 1978 *J. Fluid Mech.* **88**, 133.

CLARK, A. R. 1979 Ph.D. dissertation, University of Houston.

CLARK, A. R. & HUSSAIN, A. K. M. F. 1981 (To be submitted.)

CORCOS, G. M. & SHERMAN, F. S. 1976 *J. Fluid Mech.* **73**, 241.

CORINO, E. R. & BRODKEY, R. S. 1969 *J. Fluid Mech.* **37**, 1.

CROW, S. C. & CHAMPAGNE, F. H. 1971 *J. Fluid Mech.* **48**, 547.

DAVIES, P. O. A. L. & BAXTER, D. R. J. 1978 In *Structure and Mechanisms of Turbulence I*, Lecture Notes in Physics, vol. 75 (ed. H. Fielder), p. 125. Springer.

FOSS, J. F. 1977 *Symp. Turb. Shear Flows, Penn State Univ.*, pp. 11.33–11.42.

HUSAIN, Z. D. & HUSSAIN, A. K. M. F. 1979 *A.I.A.A. J.* **17**, 48.

HUSSAIN, A. K. M. F. & HUSAIN, Z. D. 1980 *A.I.A.A. J.* **18**, 1462.

HUSSAIN, A. K. M. F., KLEIS, S. J. & SOKOLOV, M. 1980 *J. Fluid Mech.* **98**, 97.

HUSSAIN, A. K. M. F. & THOMPSON, C. A. 1980 *J. Fluid Mech.* **100**, 397.

HUSSAIN, A. K. M. F. & ZAMAN, K. B. M. Q. 1975 In *Proc. 3rd Interagency Symp. on Univ. Res. in Transportation Noise, Univ. of Utah*, p. 314.

HUSSAIN, A. K. M. F. & ZAMAN, K. B. M. Q. 1977 *Structure and Mechanisms of Turbulence I*, Lecture Notes in Physics, vol. 75 (ed. H. Fiedler), p. 31. Springer.

HUSSAIN, A. K. M. F. & ZAMAN, K. B. M. Q. 1980 *J. Fluid Mech.* **101**, 493.

HUSSAIN, A. K. M. F. & ZEDAN, M. F. 1978 *Phys. Fluids* **21**, 1100.

KLEIS, S. J. & HUSSAIN, A. K. M. F. 1981 (To be submitted.)

KLINE, S. J., REYNOLDS, W. C., SCHRAUB, F. A. & RUNSTADLER, P. W. 1967 *J. Fluid Mech.* **30**, 741.

KO, N. W. M. & DAVIES, P. O. A. L. 1971 *J. Fluid Mech.* **50**, 49.

KOTSOVINOS, N. E. 1976 *J. Fluid Mech.* **77**, 305.

KOVASZNAY, L. S. G., KIBENS, V. & BLACKWELDER, R. F. 1970 *J. Fluid Mech.* **41**, 283.

LANDAHL, M. T. 1967 *J. Fluid Mech.* **29**, 441.

LAU, J. C. 1978 The vortex-street structure of turbulent jets. Part 2. (Submitted to *J. Fluid Mech.*)

LAU, J. C. & FISHER, M. J. 1975 *J. Fluid Mech.* **67**, 229.

LAU, J. C., FISHER, M. J. & FUCHS, H. V. 1972 *J. Sound Vib.* **22**, 379.

LAUFER, J. 1974 In *Ommagio a Carlo Ferrari* (ed. Levrotto & Bella), p. 451.

LIEPMANN, H. 1978 Experimental approaches in fluid mechanics. Invited lecture at the *8th U.S. National Cong. on Applied Mechanics, UCLA*.

MOLLO-CHRISTENSEN, E. 1967 *Trans. A.S.M.E.* E, *J. Appl. Mech.* **89**, 1.

MOORE, C. J. 1977 *J. Fluid Mech.* **80**, 321.

OSTER, D., DZIOMBA, B., FIEDLER, H. & WYGNANSKI, I. 1977 In *Structure and Mechanisms of Turbulence I*, Lecture Notes in Physics, vol. 75 (ed. H. Fiedler), p. 48. Springer.

PATEL, R. P. 1973 *A.I.A.A. J.* **13**, 245.

PETERSEN, R. A. 1978 *J. Fluid Mech.* **89**, 469.

PHILLIPS, O. M. 1967 *J. Fluid Mech.* **29**, 131.

PUI, N. K. & GARTSHORE, I. S. 1978 *J. Fluid Mech.* **91**, 111.

ROCKWELL, D. O. 1972 *Trans. A.S.M.E.* E, *J. Appl. Mech.* **39**, 883.

SAFFMAN, P. G. 1978 *J. Fluid Mech.* **84**, 625.

SOKOLOV, M., HUSSAIN, A. K. M. F., KLEIS, S. J. & HUSAIN, Z. D. 1980 *J. Fluid Mech.* **98**, 65.

TOWNSEND, A. A. 1956 *The Structure of Turbulent Shear Flow*. Cambridge University Press.

WIDNALL, S. 1975 *Ann. Rev. Fluid Mech.* **89**, 413.

WILLMARTH, W. W. & WOOLDRIDGE, C. E. 1962 *J. Fluid Mech.* **14**, 187.

WILLS, J. A. B. 1964 *J. Fluid Mech.* **20**, 417.

WILLS, J. A. B. 1970 *J. Fluid Mech.* **45**, 65.

WINANT, C. D. & BROWAND, F. K. 1974 *J. Fluid Mech.* **63**, 237.

YULE, A. J. 1978 *J. Fluid Mech.* **89**, 413.

ZAMAN, K. B. M. Q. & HUSSAIN, A. K. M. F. 1980 *J. Fluid Mech.* **101**, 449.

ZILBERMAN, M., WYGNANSKI, I. & KAPLAN, R. E. 1977 *Phys. Fluids Suppl.* **20**, 258.